JGR Atmospheres

RESEARCH ARTICLE
10.1029/2019JD031529

Assimilation of Cosmic-Ray Neutron Counts for the Estimation of Soil Ice Content on the Eastern Tibetan Plateau

Samuel Mwangi[1], Yijian Zeng[1], Carsten Montzka[2], Lianyu Yu[1], and Zhongbo Su[1,3]

[1]Faculty of Geo-information Science and Earth Observation (ITC), University of Twente, Enschede, The Netherlands, [2]Institute of Bio- and Geosciences: Agrosphere (IBG-3), Forschungszentrum Jülich GmbH, Jülich, Germany, [3]Key Laboratory of Subsurface Hydrology and Ecological Effect in Arid Region of Ministry of Education, School of Water and Environment, Chang'an University, Xi'an, China

Key Points:
- The conventional nonlinear vertical weighting approach is adherent to cosmic-ray creation and transport theory
- The applied land surface model is capable of accurately simulating the unfrozen soil water content and soil temperature
- It was possible to improve total soil water analyses and consequently enhance the quantification of soil ice content by deploying the Observing System Simulation Experiments

Correspondence to:
Y. Zeng and Z. Su,
y.zeng@utwente.nl;
z.su@utwente.nl

Citation:
Mwangi, S., Zeng, Y., Montzka, C., Yu, L., & Su, Z. (2020). Assimilation of cosmic-ray neutron counts for the estimation of soil ice content on the eastern Tibetan Plateau. *Journal of Geophysical Research: Atmospheres*, *125*, e2019JD031529. https://doi.org/10.1029/2019JD031529

Received 19 AUG 2019
Accepted 19 JAN 2020
Accepted article online 24 JAN 2020

Abstract Accurate observations and simulations of soil moisture phasal forms are crucial in cold region hydrological studies. In the seasonally frozen ground of eastern Tibetan Plateau, water vapor, liquid, and ice coexist in the frost-susceptible silty-loam soil during winter. Quantification of soil ice content is thus vital in the investigation and understanding of the region's freezing-thawing processes. This study focuses on the retrieval of soil ice content utilizing the in situ soil moisture (i.e., liquid phase) and cosmic ray neutron measurements (i.e., total water including liquid and ice), with Observing System Simulation Experiments. To derive the total soil water from neutron counts, different weighting methods (revised, conventional, and uniform) for calibrating the cosmic-ray neutron probe (CRNP) were intercompared. The comparison showed that the conventional nonlinear method performed the best. Furthermore, to assimilate fast neutrons using the particle filter, the STEMMUS-FT (Simultaneous Transfer of Energy, Mass and Momentum in Unsaturated Soil) model was used as the physically based process model, and the COSMIC model (Cosmic-ray Soil Moisture Interaction Code) used as the observation operator (i.e., forward neutron simulator). Other than background inputs from disturbed initializations in the STEMMUS-FT, model uncertainties were predefined to assimilate fast neutrons. We observed that with enough spread of uncertainties, the updated states could mimic the CRNP observation. In all setups, assimilating CRNP measurements could enhance total soil water analyses, which consequently led to the improved detection of soil ice content and therefore the freezing thawing-process at the field scale.

1. Introduction

Soil moisture is a key component in the hydrological cycle that controls the land-atmosphere water and energy interactions (Babaeian et al., 2019). In cold regions, investigation of freezing-thawing (FT) processes is essential in the understanding of the water, energy, and carbon cycles, which are key in climate studies (Li et al., 2010; Rautiainen et al., 2014; Zhao et al., 2017). Thawing of permafrost soils results in positive global warming feedback due to the release of carbon dioxide and methane (Cox et al., 2000; Li et al., 2010; Mironov et al., 2016). Soil freezing also tends to hinder infiltration thus leading to issues related to water logging, soil erosion, reduced root-water uptake, and enhanced surface runoff (Cherkauer & Lettenmaier, 1999; Schwank et al., 2004; Sheshukov & Nieber, 2011). For engineering applications, for example, design of buried pipelines and petroleum reservoirs, FT needs to be considered to mitigate against possible disasters (Civan, 2000). Accurate partitioning of soil moisture into its frozen and unfrozen components is therefore essential for effective and timely decision making in different applications.

In situ soil moisture monitoring is typically performed with sensor methods based on electromagnetic measurements of soil permittivity. However, permittivity changes drastically when the soil freezes, so that typical monitoring methods are derogated in cold regions. The use of soil moisture sensors, besides having limited spatial coverage, requires complicated procedures to partition between unfrozen and frozen water content. The current approach for obtaining soil ice content (SIC) is through the determination of unfrozen soil water content (USWC) and total soil water content (TSWC). The assumption that the USWC-apparent dielectric permittivity relationship (e.g., Topp et al., 1980) in unfrozen soils is similar to that for frozen soils (Patterson & Smith, 1981) makes the derivation of the USWC from field

observations practically possible. Measurement of TSWC, however, needs dedicated geophysical approaches, for example, using nuclear magnetic resonance (Watanabe & Wake, 2009) or gamma ray attenuation (Zhou et al., 2014) methods.

In contrast, cosmic-ray neutron probes (CRNP) (Zreda et al., 2008) measure those neutrons that are particularly sensitive to collisions with hydrogen nuclei, and therefore, they can be used to measure the concentration of hydrogen in materials at the land surface. This includes both the presence of water in vegetation, subsurface biomass and organic matter, surface water, atmospheric vapor and clay lattices water (Baatz et al., 2015), and ice. The CRNP's insensitivity to the physical state of water (Desilets et al., 2010) allows continuous monitoring of soil moisture and SIC at the field-scale averaged over several hectares in areal footprint and tens of decimeters in depth profiles (Schrön et al., 2017).

Total soil water (as inferred from CRNP measurements) exists in forms of ice, liquid, and vapor in frozen soils. Predicting the FT process, therefore, requires the use of coupled water and energy flux models that have been shown to vary in their structure (governing equations) complexities, and/or processes considered (Li et al., 2010). Simulations from such models are likely to deviate from measurements due to systematic bias (i.e., uncertainties in the forcing information, model structures, or parameterization schemes) (Yu et al., 2018). To account for these errors, data assimilation, which is defined as the integration of near-real-time observations (likelihood) with the numerical model output data (prior) to give enhanced estimates (posterior) of the evolving system states (Swinbank & O'Neill, 1994), is carried out to update model state (and/or parameter) simulations. Majority of assimilation studies (e.g., Draper et al., 2011; Han et al., 2015; Montzka et al., 2011 2012; Moradkhani, 2008; Moradkhani, Hsu, et al., 2005; Moradkhani, Sorooshian, et al., 2005; Zhang et al., 2017) have utilized measured and remotely sensed data within different assimilation frameworks. Among the assimilation algorithms, the particle filter has been found suitable for dealing with the highly nonlinear nature of soil water and heat flow models (Montzka et al., 2011; Moradkhani, Hsu, et al., 2005). The particle filter is an approach based on a set of Monte Carlo algorithms. With the particle filter, one can combine these Monte Carlo algorithms with a physically based process model, for better prediction of the evolving soil states. This improved prediction is especially true for environmental processes which exhibit random walks/variability over space and time.

In this study, a particle-filtering assimilation framework was used to assimilate observed cosmic-ray neutron counts via integrating the soil water and heat flow model and the neutron count forward simulation model, with the aim of improving the detection of SIC and the FT process on the eastern Tibetan Plateau. In the following section, other than the study area and data, the overall methodology is introduced. It begins with the CRNP and its associated calibration methods for deriving soil water content. This is then followed with the brief description of the physically based soil water and heat flow model (STEMMUS-FT, Simultaneous Transfer of Energy, Mass and Momentum in Unsaturated Soil) and the neutron count forward simulation model (COSMIC, Cosmic-ray Soil Moisture Interaction Code). Furthermore, we detail how the particle filtering assimilation framework was applied to conduct Observing System Simulation Experiments (OSSEs). In section 3, the correction of CRNP measurements, intercomparison of different weighting methods for deriving spatially representative soil water content, and calibration of the probe are presented. With the selected weighting method, the assimilation experiments were implemented to update TSWC for the detection of SIC and FT processes. Section 4 concludes this study and proposes some outlooks.

2. Materials and Methods

2.1. Study Area and Data

Maqu site is situated in the eastern Tibetan Plateau (33°30′–34°15′N, 101°38′–102°45′E) with elevations upward of 3.200 m above sea level (see Figure 1). The area experiences dry winters (coldest month: January) and rainy summers (warmest month: July) with the annual mean air temperature being 1.28 °C (Yu et al., 2018). These low temperatures, coupled with the site's frost-susceptible silty-loam soil type, make FT processes common during winter. The site is equipped with the following: soil moisture and soil temperature monitoring sensors (ECH_2O-5TM probes) at 5, 10, 20, 40, 80, and 160 cm depths; a CRNP; a 20 m planetary boundary layer tower that provides wind speed, air humidity, and temperature observations at five above-ground heights (2.35, 4.2, 7.17, 10.13, and 18.15 m); and an eddy-covariance system (Dente et al., 2012; Zheng et al., 2014).

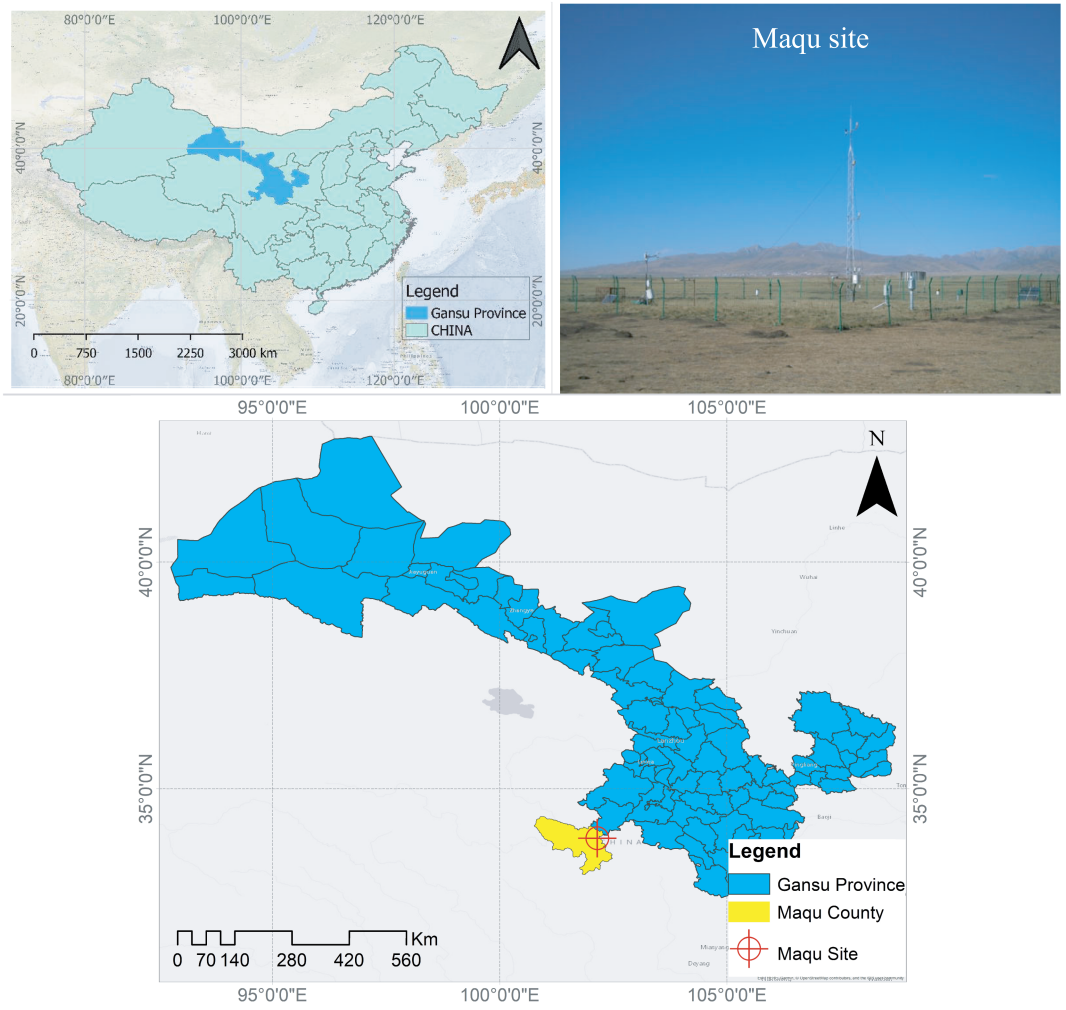

Figure 1. Maqu site (adapted from data sourced from www.itc.nl and gadm.org *via* diva-gis.org).

The key data utilized for this study is subdivided into three categories as presented in Table 1, that is, CRNP correction and calibration data, input data for the STEMMUS model, and data related to the COSMIC model. The in situ soil moisture and soil temperature measurements were treated as sources of reference information, against which simulated states were validated. Since the dielectric permittivity (ε) of ice is similar to that of dry mineral soils (i.e., 3.2 and 2.2–3.5, respectively), variations in the apparent dielectric constant tend to be dominated by variations in the unfrozen water (ε = 87.7 at 0 °C) (Patterson & Smith, 1981). During the winter season, in situ soil moisture measurements were thus taken as the "true" USWC.

2.2. Methodology

To realize the detection of SIC via assimilating CRNP measurements, we design OSSEs (section 2.2.5), which couple the soil water and heat flow model (STEMMUS-FT; section 2.2.3) and the forward observation simulator of neutron counts (COSMIC; section 2.2.2), together with the particle filtering data assimilation framework (section 2.2.4). The STEMMUS-FT provides the needed soil state inputs (i.e., USWC and SIC) for the COSMIC model, and the coupling between the two models thus enables the assimilation of neutron counts with the 1-D particle filter. It is expected that assimilating CRNP measurements will enhance total soil water analyses, which will consequently lead to the improved detection of SIC and, therefore, the FT process at the field scale. To evaluate the performance of the assimilation experiments in estimating SIC, it is necessary to first calibrate the CRNP measurements (section 2.2.1) and to derive spatially representative soil water content at the field scale.

Table 1
CRNP Correction and Calibration Data, STEMMUS Cardinal Data, and COSMIC Parameters and Input Data

Data	Unit	CRNP correction and calibration	STEMMUS	COSMIC
Cosmic ray neutron counts (N)	(cph)	√		√
Air pressure	(hPa)	√	√	
Air relative humidity	(%)	√	√	
Solar factor	(-)	√		
Precipitation	(mm/hr)		√	
Air temperature	(°C) [K]	√	√	
Wind speed	(m/s)		√	
Surface temperature	(°C) (K)		√	
Initial: soil moisture soil temperature	(m^3/m^3) (°C) (K)		√	
Hydraulic parameters: saturated hydraulic conductivity porosity, saturated and residual SWC van-Genuchten parameters (n and α)	(cm/hr) (m^3/m^3) (-) (cm^{-1})		√	
Dry soil bulk (ρ_s) and soil water density (ρ_w)	(g/cm^3)	√	√	√
High-energy neutron creation parameter (N_{he})	(-) (g/cm^2)			√
High-energy and fast neutron soil and water attenuation lengths				
Simulated soil water content (SWC)	(m^3/m^3)			√

The methodical approach of the present work is summarized in Figure 2. The moderated neutron counts as observed by the CRNP over the 2016 period (i.e., August to October 2016 for CRNP calibration and January to March 2016 for soil ice estimation) were first corrected for atmospheric pressure, air humidity, and incoming cosmic-ray effects. The conventional (both linear and nonlinear vertical) and revised weighting methods were then compared with the equally weighted approach. The selection of the most representative weighting method (for this study) was based on comparison with COSMIC derivations. The soil water data set from the field sampling campaign was averaged using the selected method and used to derive the site-specific calibration parameter (N_0). With the calibrated N_0, the averaged reference TSWC (from CRNP) was derived. Furthermore, with the selected weighting method, the USWC as observed by in situ probes could hence be averaged. The SIC (= TSWC − USWC) was consequently calculated to serve later as the reference against which the estimated SIC was assessed. The physically based process model (STEMMUS-FT) was then set up for several experiments. The model as calibrated in Yu et al. (2018) was run, and the simulated states were used further in data assimilation experiments. A sequential importance resampling particle-filtering assimilation framework (see Figure 4), which integrated STEMMUS-FT and COSMIC, was formulated for updating the modeled TSWC and thus enhanced the quantification of SIC.

2.2.1. CRNP Measurements

The CRNP is based on the principle of neutron thermalization. Hydrogen, which is present in soil water, is the most dominant element in the moderation (thermalization) of fast neutrons (Zreda et al., 2012). The probe provides above-ground moderated neutron measurements, which can be used to infer the TSWC. The most widely applied counts-to-TSWC translation model (Schreiner-McGraw et al., 2016; Schrön et al., 2017; Zreda et al., 2012) is the shape-defining function proposed by Desilets et al. (2010).

The moderated CRNP observations require correction for air pressure, air humidity, and incoming cosmic-ray radiation. This is necessary to ensure reliable inference of TSWC from the neutron counts. For the derivation of the water vapor correction factor (f_{wv}), a reference absolute humidity (ρ_{v0}^{ref}) of 0 gm^{-3} was used, while the average atmospheric pressure over the sampling period was taken as the reference (P_0 = 672.81 hPa) for the pressure correction factor (f_p). The standard approach (Hawdon et al., 2014; Rosolem et al., 2013; Zreda et al., 2012) as detailed in Appendix A was applied. Correction for biomass change was found to have a negligible contribution to the temporal cosmic ray signal (results not shown). The vegetation is alpine meadow dominated by *Kobresia pygmaea* and *Saussurea glomerata* associated with *Potentilla spp*, with a very low amount of water and biomass. Observed neutron counts also exhibit large fluctuations over time and therefore need smoothing for better comparability to the soil moisture variations. The corrected counts were therefore subjected to a *Savitzky-Golay* least squares 24-hr smoothing filter to reduce the sharp and abrupt variations over time. The *Savitzky-Golay* filter, which is based on the least squares method, was preferred as it can extract as much information as possible (Savitzky & Golay, 1964).

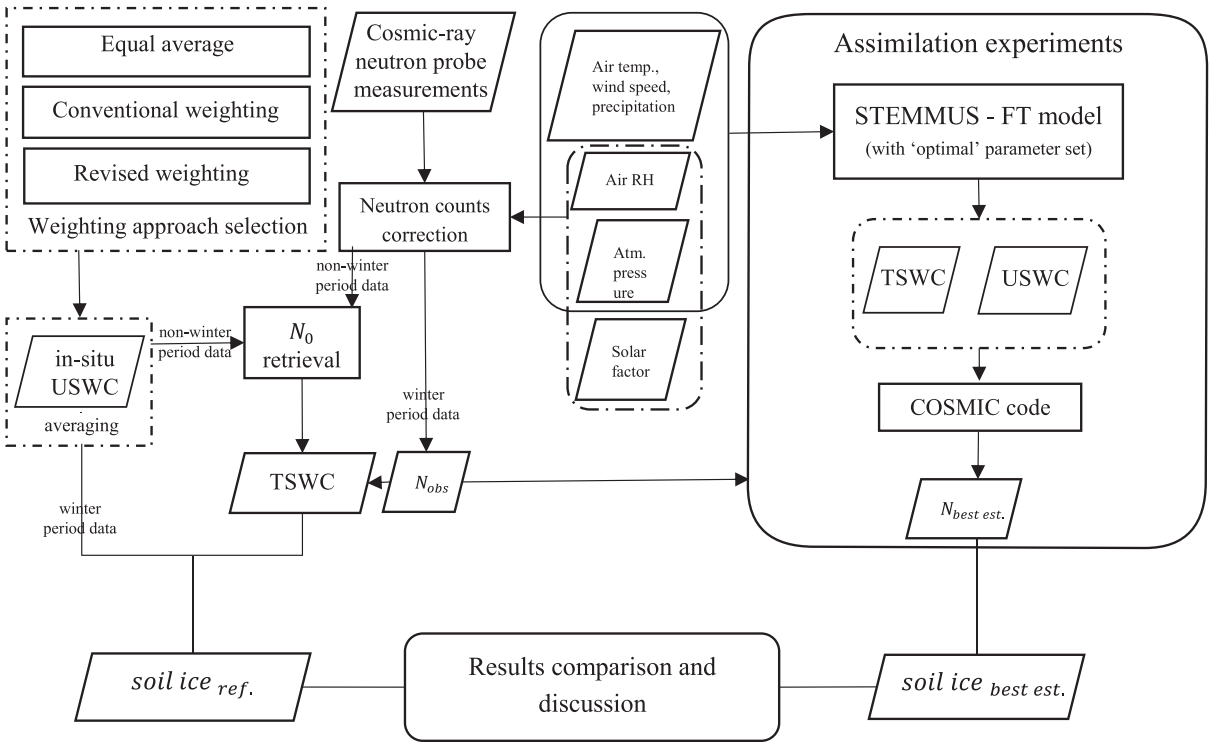

Figure 2. Flow diagram of this study (the assimilation experiments approach is detailed in Figure 4 and the weighting methods in Appendix A).

It is imperative to have the site-specific parameter (N_0) accurately calibrated before inferring soil moisture estimates from the neutron counts. To this end, different weighting approaches have been proposed for CRNP calibration, taking into account the probe's effective measuring footprint. The methods include the conventional (Franz et al., 2012), conventional nonlinear (Bogena et al., 2013), and revised (Schrön et al., 2017) approaches. Since points in the CRNP's footprint contribute differently to the measured neutron counts, different weights need to be assigned as functions of soil moisture, distance, and depth (Schrön et al., 2017). The equally weighting method has thus been replaced with the conventional and revised methods in current CRNP calibration/validation campaigns as they are based on the cosmic neutron creation and transport theory, that is, weighting is based on the contribution of fast neutron flux from different layers to the total flux over the profile (Bogena et al., 2013; Franz et al., 2012; Köhli et al., 2015; Schrön et al., 2017; Zreda et al., 2008). Appendix A summarizes the weighting approaches.

The conventional (both linear and nonlinear vertical) and revised weighting methods were compared with the equally weighted approach. The weighting methods were carried out following iteration steps summarized in Schrön et al. (2017). The sampled gravimetric soil water data set was averaged using the different weighting methods and used to derive the site-specific calibration parameter (N_0). The most representative (for this study) weighting approach was selected based on the comparison to COSMIC derivations (see section 3.1). The corrected and smoothed neutron counts together with the calibrated N_0 were then used in the Desilets et al.'s (2010) equation (Appendix A; equation (A2)) for determining the average reference total soil water. With the spatially averaged unfrozen soil water and assuming total soil water conservation (i.e., TSWC = USWC+SIC), the reference SIC was consequently calculated.

2.2.2. COSMIC Model: Forward Observation Simulator

Algorithms that derive counts from soil moisture include the Monte Carlo N-Particle eXtended neutron transport code and the much faster COSMIC (Shuttleworth et al., 2013). COSMIC assumes the existence of three dominant processes in the generation of fast neutrons, namely, (1) exponential reduction of high-energy neutrons with depth; (2) fast neutrons creation at all depths depending on number of high-energy neutrons, local density of dry soil, and local density of soil water per unit soil volume; and (3) the

proportion of fast neutrons detected above the ground is attenuated exponentially by a factor related to the distance between origin of the neutrons and the detector (Shuttleworth et al., 2013). It is expressed as follows:

$$N_{\mathrm{COSMOS}} = N_{\mathrm{he}} \int_0^{\infty} \left\{ A(z)[\alpha\rho_s(z) + \rho_w(z)] \exp\left(-\left[\frac{m_s(z)}{L_1} + \frac{m_w(z)}{L_2} \right] \right) \right\} \mathrm{d}z \quad (1)$$

where N_{he} is the high-energy neutron flux given by CN^0_{he} (C = fast neutron creation constant for pure water; N^0_{he} = number of high-energy neutrons at the soil surface); $\rho_s(z)$ is the local bulk density of dry soil, $\rho_w(z)$ the total soil water density; $\alpha = 0.404 - 0.101\rho_s$ is the relative (soil vs. water) fast neutron efficiency of creation factor; $L_1 = 161.986$ g cm^{-2} and $L_2 = 129.146$ g cm^{-2} are the high-energy soil and water attenuation lengths, respectively; $m_s(z)$ and $m_w(z)$ are the integrated mass per unit area of dry soil and water, respectively.

$A(z) = \left(\frac{2}{\pi}\right) \int_0^{\pi/2} \exp\left(\frac{-1}{\cos(\theta)} \left[\frac{m_s(z)}{L_3} + \frac{m_w(z)}{L_4} \right] \right) \mathrm{d}\theta$ is the integrated average attenuation of the neutrons generated at depth z. θ here is the angle between the vertical below the detector and the line between the detector and each point in the plane; $L_3 = -31.65+99.29\rho_s$ and $L_4 = 3.163$ g cm^{-2} are the fast neutron soil and water attenuation lengths.

During winter periods, the density of soil water should be treated as the effective density of water, considering both the densities of frozen and unfrozen phases of water. In light of this, minor modifications were made to the COSMIC code to account for the effective density of water:

$$\rho_{\mathrm{eff}} = f_L \times \rho_L + f_i \times \rho_i \quad (2)$$

$$m_w = \rho_{\mathrm{eff}} \times TSWC \quad (3)$$

where ρ_{eff} is the effective water density, f_L and f_i are the unfrozen/liquid water and ice fractions (-) respectively, ρ_L and ρ_i are the liquid and ice densities, respectively. It is assumed the L_2 and L_4 water (hydrogen) attenuation lengths (g/cm^2) are insensitive to the physical state of soil water.

The COSMIC code, as given in equation (1), requires the calibration of the high-energy neutron intensity parameter, N_{he}. To this end, observed soil moisture was used in COSMIC and the N_{he} parameter (e.g., initially set to $N_{\mathrm{he}} = 0.1612\ N_0 + 7.1956$; Baatz et al., 2014) tuned until the simulated counts converged to the observed CRNP counts. An optimal N_{he} of 654.963 was obtained. The soil moisture utilized in the calibration was from a nonwinter period when the TSWC, as observed by the CRNP, is equal to the in situ USWC, that is, ST > 0 °C. This value was consequently used as the reference N_{he} in other parts of this study where the COSMIC model was utilized.

2.2.3. STEMMUS Model: Soil FT Model

While applying the theory by Philip and De Vries (1957), traditional coupled water and energy models that simulate states in the unsaturated zone widely disregard the flow of the gas phase (Zeng et al., 2011b). Nevertheless, the gaseous phase (water vapor and dry air) flow mechanism has been shown to substantially enhance the vapor transport in arid regions (Wen et al., 2013; Zeng, 2013; Zeng, Su, et al., 2009; Zeng, Wan, et al., 2009; Zeng & Su, 2013). This has led to the development of multiphase models such as STEMMUS (Zeng et al., 2011a). In fact, the freezing processes can be analogous to drying (Farouki, 1981; Koopmans & Miller, 1966; Rautiainen et al., 2014), which renders the importance of vapor transport in frozen soil. Yu et al. (2018) found that during the freezing period, water vapor can transport from beneath the freezing front to the land surface.

The mutual dependence of soil temperature and water content makes frozen soils a complicated thermodynamic equilibrium system. The freezing effect explicitly considered in STEMMUS-FT includes three parts (Yu et al., 2018): (i) the blocking effect on conductivities (hydraulic and air permeability); (ii) thermal effect on soil thermal capacity/conductivity; and (iii) the release/absorption of latent heat flux during water phase change.

Given the prefreezing matric potential h (m) and temperature T (°C), the soil freezing temperature T_{CRIT} (°C) and the soil freezing potential are calculated as

$$T_{\mathrm{CRIT}} = T_0 + \frac{ghT_0}{L_f} \tag{4}$$

$$h_{\mathrm{Frz}} = \frac{L_f}{gT_0}(T - T_0)\cdot H(T - T_{\mathrm{CRIT}}) \tag{5}$$

L_f (J kg^{-1}) is the latent heat of fusion, g (m s^{-2}) is the gravity acceleration, T_0 (273.15 K) is the absolute temperature. H (.) is the Heaviside function (i.e., zero for negative arguments and one for positive arguments). The h and h_{Frz} are further used to determine the USWC and TSWC according to the soil freezing characteristic curve (SFCC) and soil water retention curve (SWRC), respectively (Dall'Amico, 2010; van Genuchten, 1980):

$$\theta_L(h, T) = \theta_r + \frac{\theta_s - \theta_r}{[1 + |\alpha(h + h_{\mathrm{Frz}})|^n]^m} \tag{6}$$

$$\theta_{\mathrm{tswc}}(h) = \begin{cases} \theta_r + \dfrac{\theta_s - \theta_r}{[1 + |\alpha h|^n]^m}, & h<0 \\ \theta_s, & h\geq 0 \end{cases} \tag{7}$$

where θ_L, θ_{tswc}, θ_s, and θ_r (m^3/m^3) are the unfrozen, total, saturated, and residual water contents, respectively. α is a factor related to the inverse air-entry pressure, and n, as well as $m = 1 - 1/n$, are empirical shape parameters related to the pore size distribution, which can, in turn, be determined by fitting the van Genuchten's analytical model. For the detailed governing equations of STEMMUS-FT, the reader is referred to Appendix B.

2.2.4. Data Assimilation: 1-D Particle Filter

Data assimilation schemes are based on Bayesian inference methods that combine prior information (model forecasts or background) with the likelihood function (observations) to estimate the posterior distribution (the analysis) of states and/or parameters. Analytical expressions of the posterior distribution can be derived for simple applications. For complex problems, however, they have to be approximated often using either the Kalman Filter (Kalman, 1960), its ensemble-based variant (the ensemble Kalman filter, Evensen, 1994, 2003), or the particle filter method (Gordon et al., 1993).

Particle filters are sequential Monte Carlo-based methods used in estimating the posterior distribution, where the Bayesian update step is approximated nonlinearly and can, therefore, handle non-Gaussian distributions effectively (Montzka et al., 2012). The particle filtering algorithm can handle higher statistical moments (mode and kurtosis), in addition to mean and (co) variance that are tracked in the ensemble Kalman filter (EnKF) and thus giving a relatively full representation of the posterior (Moradkhani, Hsu, et al., 2005). Furthermore, unlike the EnKF, which requires linearization of the observation operator when calculating the Kalman gain (Montzka et al., 2012), the particle filter allows the use of nonlinear observation models in their original form. In the particle filter, each ensemble member (state and parameter particle in the joint state-parameter case) is propagated forward in time using the process model:

$$x_t^{i-} = f\left(x_{t-1}^{i+}, \varphi, u\right) + \omega \tag{8}$$

where x represents the states with i being the ensemble particle. The $-$ and $^+$ superscripts represent the a priori and a posteriori estimates, respectively. The analysis ensemble from the previous time step, $t - 1$, is propagated through the process model, f, to obtain the background at time t. Forcing data (u) and model parameter (φ) particles serve as inputs. The parameter ω is an assumed model error. When observations used in approximating the posterior are proxies of the simulated states, observation models, $h(.)$, are used; that is, $y_t = h\left(x_t^{i-}, \vartheta\right) + \nu$. As such, the observation model maps the modeled state particles, x_t^{i-}, to variables equivalent to the observed measurements. Similarly, ϑ and ν denote the observation model parameter(s) and an assumed prediction error, respectively.

Particle filters estimate the posterior using discrete random particles and their associated weights (Moradkhani, Hsu, et al., 2005):

$$p(x_{1:t}|y_{1:t}) = \sum_{i=1}^{N} w_t^i \delta(x_{1:t} - x_{1:t}^i) \tag{9}$$

where w_t^i is the weight of the ith particle, N is the number of ensemble members (particles) and $\delta(.)$ is the Dirac delta function.

Since the true posterior distribution as given by Bayes' theorem is unknown, deriving particles from it is impractical. However, it is feasible to draw the particles from an importance (proposal) distribution (Montzka et al., 2012; Moradkhani, Hsu, et al., 2005). Importance weights are expressed as follows:

$$w_t^i \propto w_{t-1}^i \frac{p(y_t|x_t^i)p(x_t^i|x_{t-1}^i)}{q(x_t^i|x_{t-1}^i, y_t)} \tag{10}$$

$p(y_t|x_t^i)$ is the likelihood (a Gaussian distribution, as given by equation (12), is generally assumed for its estimation), $p(x_t^i|x_{t-1}^i)$ is the transition prior, and $q(x_t^i|x_{t-1}^i, y_t)$ is the proposal distribution. Since it is common to select the transition prior as the proposal distribution (Gordon et al., 1993; Montzka et al., 2012; Moradkhani, Hsu, et al., 2005), equation (10) reduces to

$$w_t^i \propto w_{t-1}^i p(y_t|x_t^i) \tag{11}$$

$$p(y_t|x_t^i) \approx L(y_t|x_t^i) = \frac{1}{\sqrt{(2\pi\sigma_{\text{obs}}^2)}} e^{\frac{-(y-h(x))^2}{2\sigma_{\text{obs}}^2}} \tag{12}$$

In particle filters with sequential importance resampling (SIR), only particle weights are updated. The state particles (and parameter particles in the joint state-parameter case) are resampled according to their likelihood weights (probabilities), where highly weighted particles are replicated, while those with negligible weights are discarded, that is, corresponding prior $x_t^{i=M}$ is selected as posterior such that $\sum_{i=0}^{M-1} w_i < u_i \leq \sum_{i=0}^{M} w_i$; u_i is randomly drawn from the uniform distribution over [0,1] (Gordon et al., 1993). This helps to avoid particle degeneration, which occurs when a majority of the particles exhibit negligible weight (Moradkhani, Hsu, et al., 2005).

2.2.5. OSSEs

As in equations (1)–(3), the forward observation simulator (i.e., COSMIC) needs inputs of USWC and SIC, which can be provided by a physically based soil water and heat flow model. As such, the coupling between the COSMIC model and the STEMMUS-FT model within a data assimilation framework enabled the OSSEs (Moradkhani, 2008). By translating STEMMUS-FT-simulated USWC and SIC to neutron counts (via COSMIC), CRNP field observations can be used as "observed" likelihood in assimilation schemes to correct for systematic model biases and thus improve the model estimates of neutron counts.

OSSEs are described as data assimilation implementations established to allow the examination of assimilation processes and generally involve the use of simulated data sets of terrestrial model states (Moradkhani, 2008). These data sets can be derived by running the process model with different parameterizations, initial, boundary, and/or forcing conditions. Equation (8) envisages the existence of a model error that should be able to account for the various uncertainties present in the modeling process. Most assimilation studies disregard this model error term since the assumption is that it is addressed by having considered uncertainties occasioned by forcing data, model parameters, etc. (i.e., by perturbing the model input, as well as the observations, to within their respective error ranges). For example, in Zhang et al. (2017) where a joint state-parameter assimilation was undertaken using two land surface models, a value of zero for the model error was used since it was assumed that "uncertainty was captured by uncertain model parameters and model forcings." In this study, however, arbitrary model uncertainties, in the form of random global perturbations, were also assumed to represent the existing uncertainties in parameters, structure, and forcing data. It was thus assumed that the prevailing modeling uncertainties will fall within these uncertainty ranges.

A couple of experiments were set up. The model as calibrated in Yu et al. (2018) was run over the winter period (December 2015 to March 2016) and the simulated states (Open Loop simulation results) used in further data assimilation scenarios (these scenarios begin from January 2016 as CRNP data were unavailable prior to

this date). A sequential importance resampling particle filter framework, which integrated simulated STEMMUS-FT states and COSMIC, was developed for updating the modeled TSWC and thus correcting the forecasted SIC. Having initially tested different uncertainty ranges, ± 0.1 m^3m^{-3} was determined as the limit beyond which no observable improvement could be derived (results not shown). The open-loop TSWC simulations (from STEMMUS-FT) were thus globally perturbed to have two sets of 1,000 ensemble members with uncertainty ranges of ± 0.05 m^3m^{-3} and ± 0.1 m^3m^{-3}, respectively. Global perturbation, where all modeled layers were disturbed with the same random factor as selected from within the model uncertainty ranges, was implemented to ensure that particles in the look-up table (LUT) of ensembles were consistent with model physics (i.e., conservation of the general soil water content trend in the soil column).

Illustrations of how the global perturbation was performed for the last time step while utilizing the 0.05 m^3m^{-3} and 0.1 m^3m^{-3} uncertainty ranges are given in Figures 3a and 3e. The red dotted soil water profile represents the lower bound particle, while the green dotted profile to the right is the upper bound particle. All other background particles were uniformly distributed within the two limits with a prior mean equal to the particle represented by the blue solid line. A uniform distribution was assumed because the combination of the various modeling data sets (i.e., forcing, initial, parameters) in the nonlinear model is expected to result in an unknown distribution. TSWC states from the standard 5, 10, 20, 40, 80, and 160 cm layers were then propagated through COSMIC for calculating neutron counts. These simulations were then used to derive particle weights and to perform the subsequent resampling as illustrated by Figure 4 with the CRNP observations perturbed following Poisson statistics (Zreda et al., 2012).

2.3. Performance Assessment

Objective functions used for the assessment of the results obtained from various aspects of this study include the root mean square error/difference (RMSE/D), Nash Sutcliffe Efficiency (NSE), standard deviation (σ), and correlation coefficient (CC). The RMSE and NSE statistical measures are expressed as follows:

$$RMSE/D = \left[\frac{1}{N}\sum_{i=1}^{N}\left(X_s^i - X_r^i\right)^2\right]^{0.5} \tag{13}$$

$$NSE = 1 - \frac{\sum_{i=1}^{N}\left(X_s^i - X_r^i\right)^2}{\sum_{i=1}^{N}\left(X_r^i - \overline{X_r}\right)^2} \tag{14}$$

The unbiased RMSE/D (i.e., $centered\ RMSD = \left[\frac{1}{N}\sum_{i=1}^{N}\left(\left(X_s^i - \overline{X_s}\right) - \left(X_r^i - \overline{X_r}\right)\right)^2\right]^{0.5}$) is used in Taylor diagrams to meet the cosines condition ($RMSD_{s,r}{}^2 = \sigma_s^2 + \sigma_r^2 - 2\sigma_s\sigma_r CC_{s,r}$) inherent in the geometric design of the diagrams (Taylor, 2001); where X_s and X_r are the model (simulations/analyses) and reference variables, respectively; N is the data series' population size; $\overline{X_r}$ and $\overline{X_s}$ denote the mean values.

3. Results and Discussion

3.1. Calibration of CRNP for Soil Moisture Estimates

The selection of the most representative weighting method was based on comparison to the COSMIC-based weighting approach. COSMIC calculates fast neutrons created at all depths (see section 2.2.2), and as such, can calculate the fast neutrons (from a specific depth/layer)-to-total neutron flux fraction, within the effective footprint of the CRNP. This fraction can serve as the weighting factor for each soil layer used to provide inputs to COSMIC. Consequently, these weighting factors can be used to average the in situ soil moisture measurements. Such COSMIC-based weighting approach can be considered to have roots in the cosmic neutron creation and transport theory. It is therefore assumed that the COSMIC-weighting approach can be taken as the "reference."

It was necessary to compare different weighting methods to establish the most representative weighting scheme for calibrating the CRNP at our site. To facilitate the intercomparison of the methods, one profile of detailed soil moisture measurements (down to 160 cm) near the CRNP was used (note that soil

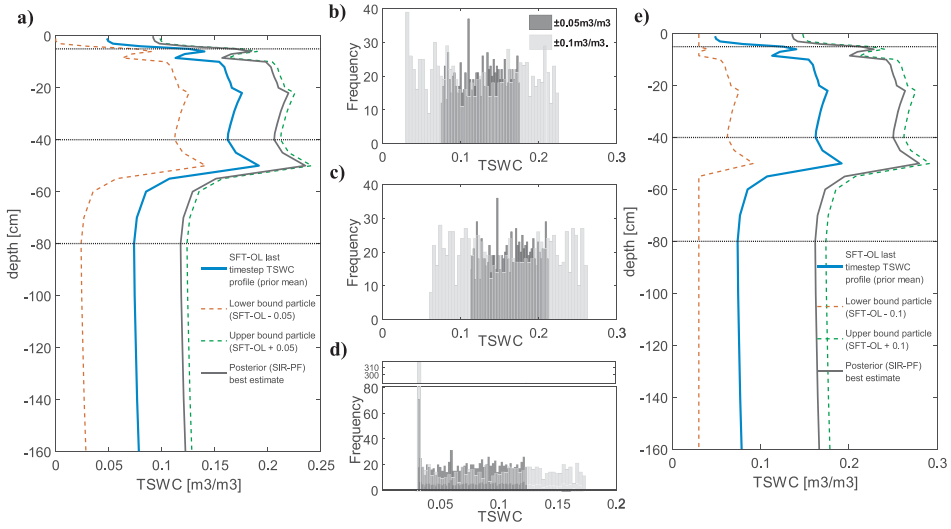

Figure 3. Example illustrating the application of the (a) ±0.05 m^3m^{-3} and (e) ±0.1 m^3m^{-3}uncertainty range global perturbation together with histograms for prior ensembles generated for the (b) 5 cm, (c) 40 cm, and (d) 80 cm layers (last simulation time-step).

moisture and CRNP observations over the August to October 2016 period [nonwinter period] were used here). The averaged soil moisture derived using the different weighting/averaging methods were compared against the COSMIC-weighting-derived soil moisture averages. Whereas the conventional and revised weighting methods attained NSE coefficients of 0.98 and 0.97 and RMSEs of 0.003 m^3 m^{-3} and 0.004 m^3 m^{-3}, respectively, the equally weighted method achieved an RMSE of 0.038 m^3 m^{-3} and an NSE of −1.67, which is way below the satisfactory threshold (0.6). Figure 5a shows statistical metrics for the different averaging methods as compared to COSMIC-based "reference." It is

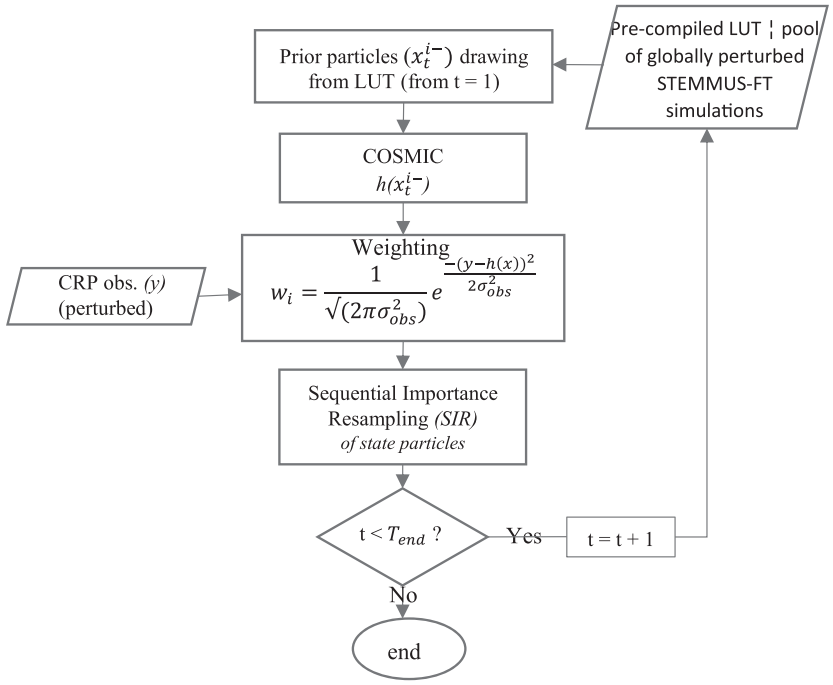

Figure 4. Data assimilation scheme (Particle Filter flow diagram) utilizing a precompiled look-up table (adapted from Moradkhani, Hsu, et al., 2005; Montzka et al., 2011).

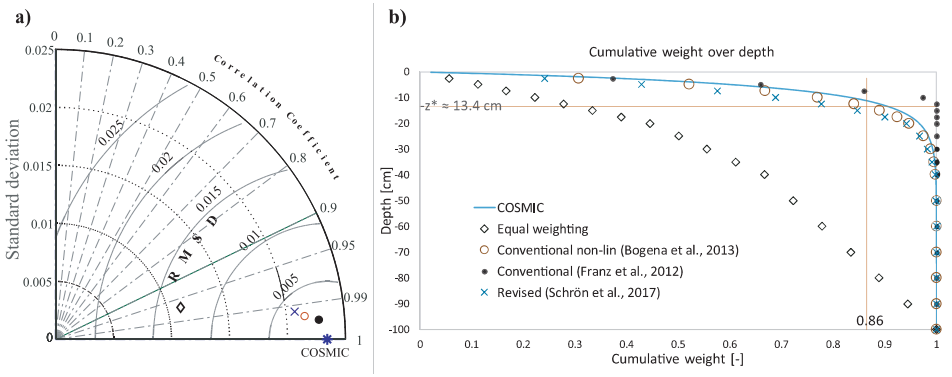

Figure 5. (a) Taylor diagram showing comparison of COSMIC-derived soil water with those from equal, conventional, and revised weighting approaches over the August to October 2016 period; (b) cumulative weights over depth (COSMIC compared to uniform, conventional [linear and nonlinear vertical], revised approaches) (Observed SWC-11·10·2016 23:45). Key applies to both figures.

evident from Figure 5b that the conventional nonlinear averaging method assigns weights similar to the COSMIC method with approximately $1 - 1/e^2$ being assigned to the uppermost layers (above Z^* = 13.4 cm). By assigning equal weights to all layers, the uniform method underestimates the weights of the upper soil layers while overestimating the weights of deeper layers and was therefore not recommended in this study. From COSMIC, 86% of the counts originate from above ~13 cm, while only ~30% originate from above (hence ~70% from below) the same depth in the uniform method.

For retrieval of the site-specific calibration parameter (N_0), calibration data from a field campaign that followed the sampling scheme method by Zreda et al. (2012) was used. Collection of data sets from 18 profiles at radii of 25 and 75 m from the CRNP (at depths ranging from 0–40 cm) was undertaken on 10 October 2016 (further details in Peng, 2017). The conventional, conventional nonlinear vertical, and the revised approaches were used to derive footprint soil moisture averages of 0.4777 $m^3\ m^{-3}$, 0.4049 $m^3\ m^{-3}$, and 0.4267 $m^3\ m^{-3}$, respectively. It is to note the uniform (equal) averaging method (0.3361 $m^3\ m^{-3}$) underestimates heavily the effective depth soil moisture content. With these averages, site-specific parameters unique to each method were calculated.

To select between the revised and conventional averaging methods, the soil moisture inferred from the CRNP observations over the August to October 2016 period was taken as the reference for intercomparisons. Specifically, three sets of soil moisture inferred from COSMIC-simulated counts were compared against the reference sets. These sets were derived by utilizing the unique revised and conventional (linear and nonlinear) site-specific parameters in equation (A2). The conventional (nonlinear vertical) approach yielded the lowest RMSE (0.063 $m^3\ m^{-3}$) and its N_0 (i.e., 3,939.38 cph) was thus adopted for other parts of this study. Selection of the conventional nonlinear method is in line with Baatz et al. (2015) on that the averaging approach considers and assigns weights similar to the COSMIC operator. The relatively high RMSE (compared to the RMSE calculated with COSMIC-weighting soil moisture averages as reference) is likely due to the use of only one in situ measurement profile to simulate neutrons for the slightly heterogeneous CRNP footprint. This is however not expected to affect inferences made from observed neutron counts because the calibrated site-specific parameters, by virtue of having been derived from field-sampled soil moisture data, already incorporate characteristics from the footprint. These intercomparisons were purely meant to determine which site-specific parameter, when used with both simulated and observed neutron counts, ensured consistent retrievals.

Reference SIC was taken as the difference between the TSWC (i.e., from CRNP) and the averaged in situ soil moisture measurements as the USWC. The USWC over the sensing depths were weighted using the selected conventional nonlinear vertical method. The "reference" SIC for the January-to-March 2016 winter period is illustrated in Figure 6.

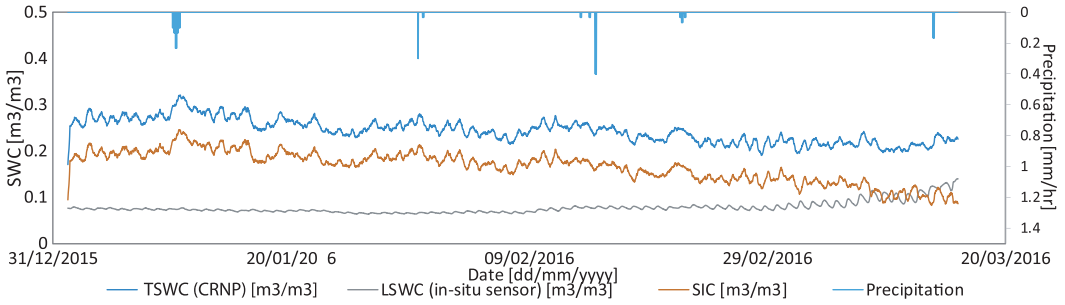

Figure 6. Soil ice "truth" time series as well as the average total soil water inferred from CRNP corrected counts and average liquid soil water derived by averaging in situ soil moisture observations using the conventional nonlinear weighting method.

3.2. STEMMUS-FT Open Loop Simulation

Figure 7 shows the STEMMUS-FT-simulated USWC, averaged using the conventional nonlinear method. Only results from January 2016 are presented herein as CRNP observations were unavailable before this date. The simulated average USWC over the CRNP's effective sensing depth yielded a positive correlation of 0.96 to the observed average with an RMSE of 0.004 $m^3\ m^{-3}$ and an NSE of 0.89. The model shows capability of simulating USWC below 0.1 $m^3\ m^{-3}$ with relatively good accuracy while largely overestimating USWCs above 0.1 $m^3\ m^{-3}$ (i.e., $RMSE_{0.1\uparrow} = 0.011\ m^3\ m^{-3}$; $RMSE_{0.1\downarrow} = 0.003\ m^3\ m^{-3}$). Since the effective depth as determined by the conventional nonlinear method consists mainly of topsoil layers, a possible explanation for this observation is the overestimation of USWC by the model at the 10 cm layer for soil temperatures above −2 °C, when the soil is experiencing transitional period. This is also the cause of fluctuations of the goodness of fit as described by the NSE at the top layers. Furthermore, Table 2 shows that the RMSEs of the USWC and soil temperature indicate better model performance with depth. This pattern, however, is disrupted at the 40 cm soil layer, which is due to the sharp soil texture change at this depth as reported by Yu et al. (2018). The soil texture change is also the likely cause of inconsistencies observed in the 40 cm layer's soil freezing characteristic curve, which determines the soil moisture and temperature dynamics in the frozen soil. The performance of the model at the 40 cm layer is therefore regarded inconclusive as it is assessed against in situ observations that also exhibit inconsistencies at this sensing depth. Since past observations have already been made, recalibration of the sensor at this depth can only be expected to improve future analyses.

During the soil freezing/thawing transition period, the soil suffers from frequent freeze/thaw cycles and the heat exchange is significant, which leads to observable changes in soil hydraulic/thermal properties. Such changes in soil hydrothermal properties make it difficult to mimic the water and heat transfer during transition periods, especially when the current existing freeze-thaw models/theories do not consider comprehensively all these effects (Yu et al., 2018). Nevertheless, the STEMMUS-FT model shows quite good capability of accurately simulating soil temperatures and the USWC; the assimilation experiments were therefore only set up to update the TSWC and consequently, the SIC. The assimilation scheme was also univariate in nature; hence, only the CRNP measurements (proxy of TSWC) were assimilated.

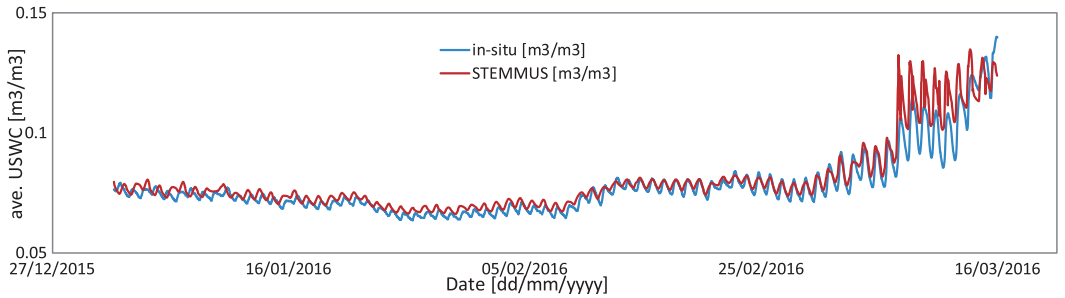

Figure 7. Average USWC applying the conventional nonlinear method (average for the CRNP footprint).

Table 2
Simulated-Versus-Observed States RMSE and Correlation Coefficients

Depth (cm)	RMSE		NSE		*r*	
	USWC (m^3/m^3)	ST (°C)	USWC	ST	USWC	ST
5	0.011	1.34	0.825	0.582	0.909	0.793
10	0.006	0.82	0.778	0.758	0.971	0.891
20	0.003	0.29	0.819	0.934	0.990	0.969
40	0.006	0.61	−0.040	0.243	0.946	0.989
80	0.002	0.12	0.938	0.926	0.979	0.983

3.3. OSSEs Results With Global Perturbation

The STEMMUS-FT open-loop (SFT-OL) simulations of TSWC were globally perturbed to have two sets of 1,000 ensemble members with uncertainty ranges of ±0.05 m^3 m^{-3} and ±0.1 m^3 m^{-3}, respectively. The global perturbation altered all model layers with the same random factor, as selected from within the model uncertainty ranges. This perturbation was implemented to generate the LUT of particles that were consistent with model physics (e.g., the profile distribution pattern of soil moisture was kept to ensure the conservation of the general soil water content trend in the soil column). The globally perturbed TSWC states, derived using the method described in section 2.2.5, were propagated through COSMIC for calculating neutron counts. The COSMIC-derived simulations were then used for deriving particle weights and for subsequent resampling in the sequential importance resampling-particle filter (SIR-PF) implementation.

The simulated counts time series (based on the open-loop TSWC) is relatively constant over a large part of the simulated winter period. The small variations can be attributed to the effective density modifications made to the COSMIC code to account for the presence of frozen and unfrozen soil water. The open-loop counts do not however follow the CRNP measurements as can be observed in Figure 8

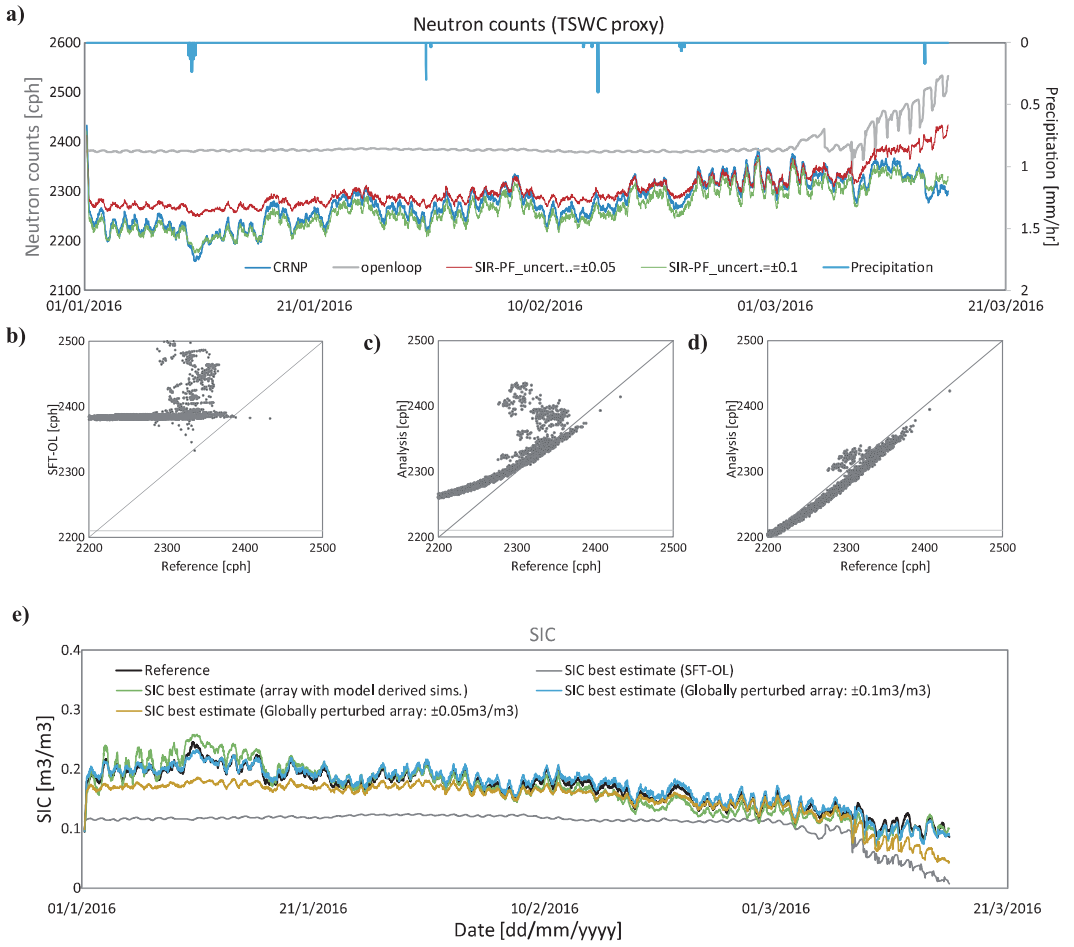

Figure 8. (a) Neutron counts time series: simulated open loop, after the implementation of SIR_PF (with ±0.1 m^3 m^{-3} and ±0.05 m^3 m^{-3} uncertainty ranges) and observed; (b) open-loop, (c) analysis ±0.05 m^3 m^{-3}, and (d) analysis ±0.1 m^3 m^{-3} scatter plots; (e) SIC averages from the different scenarios, for qualitative comparison with the reference. SIC best estimate as derived in section 3.4 is also added for comparison.

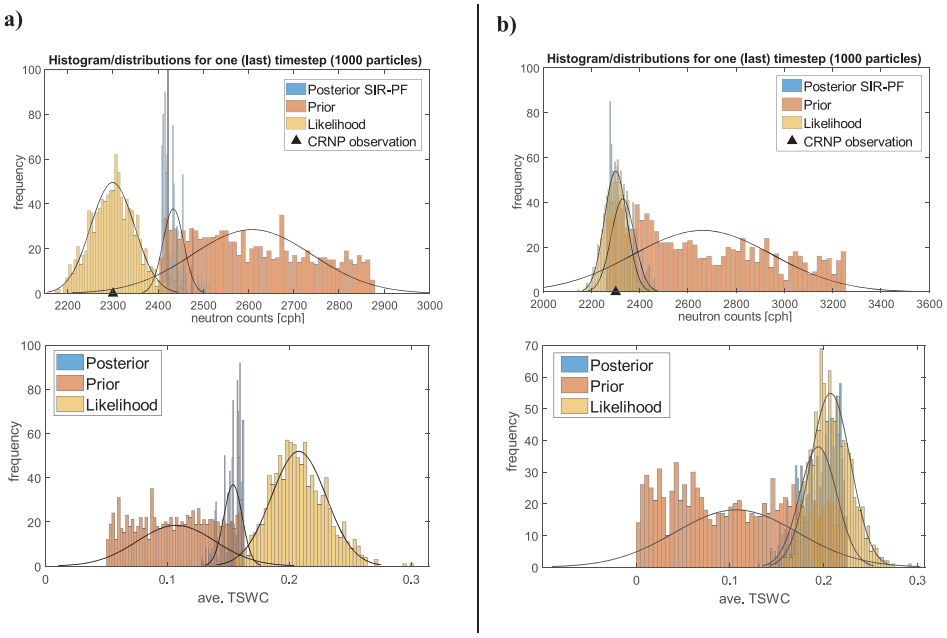

Figure 9. Posterior, prior, and likelihood histograms for the last time step (neutron counts and average TSWC, respectively): (a) ± 0.05 m^3 m^{-3} and (b) ± 0.1 m^3 m^{-3} uncertainty ranges.

due to the model's underestimation of average TSWC over the effective sensing depth of the CRNP (TSWC results not shown). Rainfall, which acts as a source of hydrogen, has an effect on the neutron counts as all precipitating events lead to an observable reduction (moderation) of counts reaching the CRNP. Furthermore, the more pronounced variations in the observed neutron counts time series suggest the potential existence of other hydrogen sources that need further investigation.

Assimilating the observed neutron counts allowed the correction and update of the simulated states as shown in Figure 8a. It is clear that with the uncertainty range of ± 0.1 m^3 m^{-3}, the updated neutron counts are in agreement with the CRNP measurement, which is much better than the results with the uncertainty range of ± 0.05 m^3 m^{-3}. The ± 0.05 m^3 m^{-3} uncertainty range (Figure 8c) attained a correlation, RMSE (i.e., difference between analyses and observations) and NSE of 0.83, 35.029 cph, and 0.368, respectively for the neutron counts (i.e.,
0.852, 0.019 m^3 m^{-3} and 0.404, respectively for the average TSWC). On the other hand, the ± 0.1 m^3 m^{-3} uncertainty range (Figure 8d) achieved a correlation of 0.983, RMSE of 15.027 cph and NSE of 0.884 for the neutron counts (i.e., 0.984, 0.008 m^3 m^{-3}, and 0.898, respectively, for the average TSWC). Both show a clear improvement when compared to the open-loop (Figure 8b) where neutron counts resulted in an r, RMSE, and NSE of 0.358, 120.758 cph, and -6.508, respectively (i.e., 0.409, 0.061 m^3 m^{-3} and -4.808, respectively, for the average TSWC).

Figure 9 illustrates the last time step's histograms for the two global perturbation scenarios where the ± 0.1 m^3 m^{-3} uncertainty range gave an estimate very close to the CRNP observation (i.e., analysis ensemble mean = 2,329.16 cph, while CRNP observation = 2,300.38 cph). This is mainly because the larger uncertainty range provided enough spread that allowed resampling of most of the posterior from prior particles close to the likelihood (i.e., resampling was mostly from particles in the 2,250–2,450cph range). The ± 0.05 m^3 m^{-3} prior distribution returned an updated best estimate of 2,434.11 cph. This deviation is the result of too narrow spread of prior particles, which cannot capture/overlay the likelihood of CRNP observations. It is interesting to observe that the last time step's soil water profile estimates for both scenarios (Figures 3a and 3e) were close to the upper limit. This should be expected as the open-loop model underestimates the TSWC toward the end of the simulation period while the CRNP observations show a downward trend (i.e., more soil water, see Figure 8a), thus the filter assigned higher weights to particles closest to the upper bound.

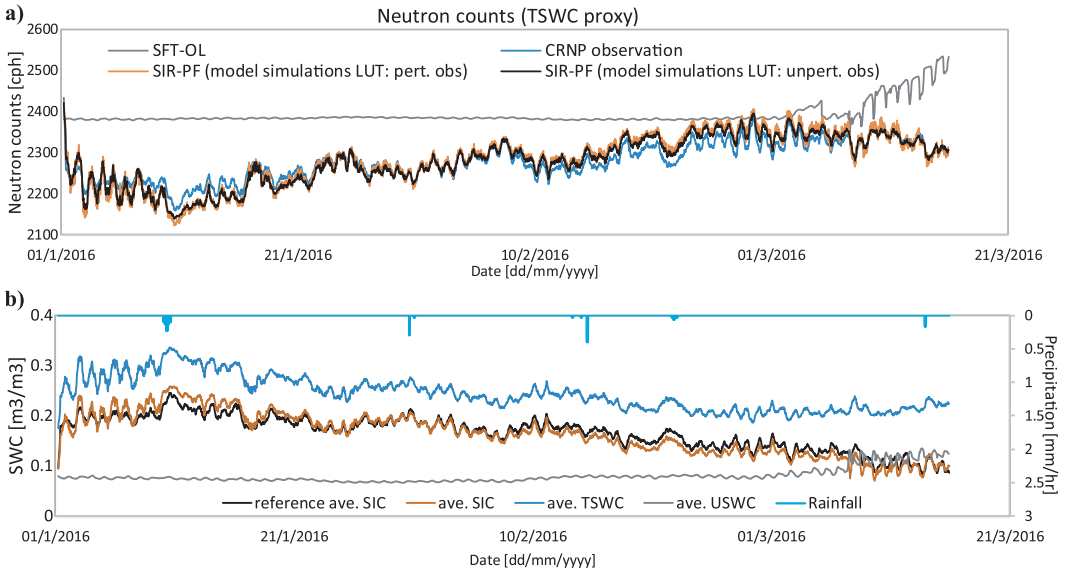

Figure 10. (a) Neutron counts time series for analyses utilizing LUT model generated particles, using perturbed and unperturbed likelihood, open-loop and CRNP observations; (b) Average TSWC (inferred from neutron counts analyses —using perturbed likelihood), USWC, and SIC best estimates.

For consistency in comparison with the reference, the TSWC from the updated neutron counts was derived by substituting the updated counts into equation (A2). Similar to derivations in section 3.1, the average USWC was derived by using the conventional nonlinear method. Assuming total soil water conservation, the best estimate of SIC could thus be derived. Similar to the TSWC, the model, as depicted by the open-loop, underestimated the SIC. The DA updates were able to reduce this with the r^2 being enhanced from 0.54 (OL) to 0.84 ($\pm$0.05 m^3 m^{-3} model uncertainty range) and 0.96 (for the $\pm$0.1 m^3 m^{-3} model uncertainty range). The goodness of fit, therefore, improved with spread. As with the TSWC updates, the $\pm$0.1 m^3 m^{-3} uncertainty range provided a fairly broad spread that allowed close tracking of the observed SIC as derived from neutron-inferred average TSWC and averaged USWC from in situ sensors. The RMSEs are 0.063, 0.021, and 0.007 for the open-loop, $\pm$0.05 m^3 m^{-3} and $\pm$0.1 m^3 m^{-3} scenarios, respectively.

3.4. OSSEs Results With Perturbed Model Physics

To generate the LUT utilized for this subsection, the initial soil water content states were perturbed with an uncertainty range of $\pm$0.1 m^3 m^{-3}. A LUT of ensembles with 1,000 particles was compiled after enough fully converged simulation data sets from the model realizations were available. Since perturbation of observations led to sharp variations of the analysis estimate, the unperturbed CRNP observations (i.e., using unperturbed CRNP counts in the particle filter weighting) were also used to evaluate whether this could allow improved corrections and smooth gradients over concurrent updating periods.

The unperturbed CRNP observations (i.e., where all 1,000 likelihood particles for each time step were set to the observed value) were used as likelihood against which the prior particles were weighted (see equation (12)). This resulted in a correlation of 0.96 (RMSE: 19.693 cph), a marginal improvement from a correlation of 0.95 (RMSE: 24.261 cph) when perturbed CRNP measurements were utilized in the particle filter weighting. An enhancement of the shape could be observed as quantified by the NSE, that is, from 0.697 to 0.801 (perturbed and unperturbed likelihood, respectively). The average SIC estimates illustrated in Figure 10b (also compared to the reference and other scenarios in Figure 8e), resulted in an RMSE, NSE, and correlation of 0.015 m^3 m^{-3}, 0.79, and 0.96, respectively. Enough spread in initial conditions, therefore, led to broadly spread simulations that could allow the likelihood (reference) to be tracked with relative accuracy similar to scenarios in the preceding section. Though the use of unperturbed measurements in the weighting step seems to slightly outperform the perturbed likelihood, the latter cannot be viewed as

inferior as there was no marked difference between the two outcomes. This finding concurs with Evensen (2003) who pointed out that whether one updates using perturbed or the first-guess observation is an arbitrary decision. That notwithstanding, Evensen (2003) recommended the use of perturbed observations since that allows the creation of ensembles with correct error statistics.

4. Summary and Conclusions

In this study, we propose a method to improve soil ice derivations by assimilating cosmic-ray observations in Maqu, Tibetan Plateau. This has potential use in agriculture, feasibility studies for effective engineering design, and climate change studies. Since soil ice impedes infiltration while the thawing also alters the soil structure, the results from this study can aid in quantifying the freezing extent and thus advise on measures to ensure perennial vegetation are not adversely affected during the cold season. When building structures, such as transport and pipeline systems, FT processes should be considered to ensure the designs can properly adapt during the cold period and thus mitigate risks and minimize maintenance costs arising in the event of damages. The release of greenhouse gases (methane and carbon dioxide) during the thawing period also contributes to global warming. Determining the soil ice and thus thawing extent should therefore be of key importance in climate change studies especially in the Tibetan Plateau whose thermodynamic processes influence the atmosphere and climate of the Northern Hemisphere (Zhou et al., 2009).

The plausibility of using the uniform averaging approach in calibrating the cosmic-ray probe was first investigated. This was done by comparing the approach to the conventional (both linear and nonlinear vertical) and revised weighting methods and validating against weighting derived from the COSMIC model. The selected weighting approach was then used to average the previously collected and compiled gravimetric soil moisture data sets for calibrating the CRNP. Using the observed neutron counts (TSWC proxy), the tuned site-specific parameter and the in situ probe (USWC) measurements, the reference ("true") SIC was derived. The STEMMUS-FT model was then used in assimilation scenarios to derive SIC best estimates. This was done by first compiling data pools that were afterward used as background data sets in a scheme that utilized the sequential importance resampling-particle filter algorithm.

The use of the equal (uniform) weighting method in calibrating the cosmic-ray probe site-specific parameter and in averaging soil water in the soil profile was found to be inappropriate, as it is not based on the fast neutrons creation and transport theory. The conventional nonlinear averaging method as proposed in Bogena et al. (2013), which was able to assign weights similar to the COSMIC model, was demonstrated to be the most suitable and consequently applied in this study. The gravimetric sampling data set used in the CRNP's calibration was collected from several points in the footprint and thus included horizontal weighting. This is however not the case for the single point soil moisture probe used in analyzing the weighting methods, which only allowed vertical weighting (horizontal weight = 1 hence neglecting spatial heterogeneity). Additional probe data series' within the CRNP's footprint should be considered in future. Nevertheless, it will not affect the selection of the weighting method for our study, considering the homogeneity of the Maqu site (Su et al., 2011; Zeng et al., 2016).

With a properly calibrated model, the soil temperature states can be accurately modeled and by applying the tuned soil freezing curve, the USWC simulations could be derived. The total soil water as simulated by the open-loop model, however, did not follow the observed trend as depicted by the cosmic-ray neutron observations. Several assimilation experiments were therefore implemented to correct the bias in the total soil water, which led to the better estimates of SIC.

By applying Bayesian inference, where cosmic-ray neutron observations were assimilated through a particle filter scheme, simulations of TSWC could be improved. This consequently led to the improvement of SIC simulations given that the model did provide accurate liquid soil water states. The assimilation experiments showed that the selection of model uncertainty range to represent various modeling biases (uncertainties in model structure, forcing data, boundary conditions, etc.) influenced the outcomes. The $\pm 0.1\ m^3\ m^{-3}$ uncertainty range allowed close tracking of the TSWC observations as inferred from the assimilation results since it provided enough spread. Similarly, the use of the data pool compiled from model run simulations also resulted in improved neutron counts analyses and thus the TSWC averages.

Drawing particles from precompiled data pools for the particle filtering implementation is appropriate for testing the scheme but a fully coupled implementation, where previous time step's posterior ensemble members are propagated through STEMMUS for deriving the current time step's priors is recommended. Nevertheless, the tremendous computation time (≈600 hr) for running this fully coupled assimilation is the main challenge to address in the near future.

Furthermore, the long-term CRNP measurements at different climate regions over Tibetan Plateau should be explored to evaluate the stability of the proposed method and its ability to be extrapolated to larger areas. It is expected that with the current approach, it will be relatively "easier" to monitor the FT states of Tibetan Plateau when compared to the effort of installing soil moisture and soil temperature networks (Su et al., 2011; Zeng et al., 2016), considering the harsh field conditions at this high-altitude cold region.

Appendix A: CRNP Counts Correction, Counts-to-TSWC and Weighting Methods

- Moderated counts correction using standard approaches (Hawdon et al., 2014; Rosolem et al., 2013; Zreda et al., 2012) is implemented as follows;

$$N_{\mathrm{corr}} = N_{\mathrm{mod}} \times f_{\mathrm{wv}} \times f_p \times f_i \tag{A1}$$

where N_{corr} (counts per hour, cph) is the corrected counts, N_{mod} (cph) is the moderated counts measured by the probe. $f_{\mathrm{wv}} = 1 + 0.0054\left(\rho_{v0} - \rho_{v0}^{\mathrm{ref}}\right)$ [-] is the relative humidity variation correction factor: ρ_{v0} (g m^{-3}) is the absolute humidity and ρ_{v0}^{ref} (g m^{-3}), the reference absolute humidity. $f_p = \exp\left[\frac{P-P_0}{L}\right]$ (-) is the atmospheric pressure variation correction factor: P (hPa) is the measured air pressure, P_0 (hpa) is the reference atmospheric pressure, and L (g cm^{-2}) is the mass attenuation length for high-energy neutrons (value varies between ~128 g cm^{-2} and ~142 g cm^{-2} at high latitudes and the equator, respectively, Zreda et al., 2012). $f_i = \frac{I_{\mathrm{ref}}}{I}$ (-), the incoming cosmic-ray correction factor: I is the selected neutron monitor counting rate at any time while I_{ref} is a reference counting rate for the same monitor at a fixed time.

- Desilets et al. (2010) shape-defining function (corrected counts to total soil water);

$$\theta(\mathrm{N}) = \frac{\mathrm{a_0}}{\left(\frac{\mathrm{N_{corr}}}{\mathrm{N_0}}\right) - \mathrm{a_1}} - \mathrm{a_2} \tag{A2}$$

θ (m^{3}m^{-3}) denotes the volumetric soil water after accounting for the soil bulk density, $a_0 = 0.0808$, $a_1 = 0.372$, and $a_2 = 0.115$ are the soil water dependence of near-surface intensity parameters, and N_0 (cph) is the site-specific calibration parameter.

- Soil Water Averaging
- Uniform (Equal) Weighting

The general averaging equation as given below is applied;

$$\theta_{\mathrm{ave}} = \frac{\sum_{i=1}^{n} w_i \theta_i}{\sum_{i=1}^{n} w_i} \tag{A3}$$

where θ_i (m^{3}m^{-3}) is the soil water content at layer i for a given profile, n is the combined number of layers in all soil sampling profiles, and w_i is the weight assigned to layer i (w_i is equivalent to $1/n$ in the equally weighted approach).

- Conventional Weighting

This is based on the weighting functions from Franz et al. (2012). The averaging iteration is implemented using equations (A4) and (A5) until convergence to a user-defined range is attained. The weights for the

sampling layers and profiles are assigned based on the depth from the surface and distance from the CRNP, respectively.

$$w_d^{\text{conv}} = \begin{cases} 1-d/D^{\text{conv}}, & d \le D^{\text{conv}} \\ 0, & d > D^{\text{conv}} \end{cases} \tag{A4}$$

$$w_r^{\text{conv}} = \begin{cases} e^{-r/127}, & r \le 300 \text{ m} \\ w_{r=300}^{\text{conv}}, & r > 300 \text{ m} \end{cases} \tag{A5}$$

where w_d^{conv} (-) is the vertical weight for each layer at depth d (cm) in a profile, $D^{\text{conv}} = z^* = 5.8/(H_p + 0.0829)$ (cm) is the effective measurement depth of the CRNP with $H_p = \frac{\rho_{bd}}{\rho_w}(\tau + soc) + \theta$ being the hydrogen pool present in the soil profile, that is, volumetric soil moisture (θ), gravimetric lattice (τ), and soil organic water (soc). ρ_{bd} and ρ_w are the bulk soil and water densities, respectively. The parameter w_r^{conv} is the horizontal weight for each profile and r (m) is the distance from the sampling profile to the CRNP probe.

The nonlinear conventional method, as proposed in Bogena et al. (2013) and recommended herein (preferred after comparing with the uniform and revised methods), computes the Cumulative Fraction of Counts (CFoC) over the vertical profile nonlinearly and ensures that some weights are assigned to layers below the effective depth (z^*) with the bottom getting the residual. Similarly, equation (A5) derives the horizontal profile weights.

$$w_d^i = \begin{cases} CFoC_1, & \text{for topsoil layer } i = 1 \\ CFoC_i - CFoC_{i-1}, & \text{for other layers; from } i = 2, ..., b-1 \\ 1-\sum_{i=1}^{b-1} w_d^i, & \text{for the bottommost layer } b \end{cases} \tag{A6}$$

where $CFoC_i = 1-e^{-d_i/\gamma}$ is the CFoC for the ith layer at depth d_i and $\gamma = -5.8/(\ln(0.14) \times (H_p + 0.0829))$.

- Revised Weighting

The conventional method assumes similar penetration depths of detected counts for all distances r from the sensor. To address this shortcoming, Schrön et al. (2017) proposed the revised averaging approach. Similar to the conventional approach, the averaging is implemented iteratively until the predefined convergence criteria is fulfilled.

$$w_d = e^{-2d/D_p} \tag{A7}$$

$$w_r = \begin{cases} \left(F_1 e^{-F_2 r^*} + F_3 e^{-F_4 r^*}\right)\left(1-e^{-F_0 r^*}\right), & 0 \text{ m} < r \le 1 \text{ m} \\ F_1 e^{-F_2 r^*} + F_3 e^{-F_4 r^*}, & 1 \text{ m} < r \le 50 \text{ m} \\ F_5 e^{-F_6 r^*} + F_7 e^{-F_8 r^*}, & 50 \text{ m} < r < 600 \text{ m} \end{cases} \tag{A8}$$

w_d (-) is the layer vertical weight; $D_p(\text{cm}) = \frac{1}{\rho_{bd}}\left(p_0 + p_1\left(p_2 + e^{-p_3 r^*}\right)\frac{p_4+\theta}{p_5+\theta}\right)$ is the revised penetration depth which varies slightly from the effective measurement depth (z^*); p_i are horizontal weighting parameters as given in Schrön et al. (2017); F_i are parameter functions as given in Schrön et al. (2017); r^*(m) is the rescaled distance (r as a function of air pressure, vegetation height, and soil moisture).

The revised and conventional (linear and nonlinear vertical) weighting iteration steps are summarized below (for more details see Schrön et al., 2017):

1. Estimate initial value (taken as the uniform average over all profiles and layers (θ)).
2. Calculate the penetration depth for each profile (D^{conv} or D_p)
3. Derive the weighted average for each profile (θ_p) by vertically averaging the layers' soil moisture values.
4. Weight the profiles (θ_p) for derivation of the horizontal footprint average (θ).
5. With the new θ, repeat 1–5 until convergence to within the user-defined criteria (1e−6 in this study) is attained.

Appendix B: STEMMUS-FT Model

The STEMMUS (Simultaneous Transfer of Energy, Mass and Momentum in Unsaturated Soil), detailed in Zeng (2013), Zeng and Su (2013), and Zeng et al. (2011a, 2011b), was extended to take into account the soil freeze-thaw process (STEMMUS-FT). The governing equations are detailed below.

B.1. Soil Water Transfer

$$\begin{aligned}\frac{\partial}{\partial t}(\rho_L\theta_L+\rho_V\theta_V+\rho_i\theta_i) &= -\frac{\partial}{\partial z}(q_{Lh}+q_{LT}+q_{La}+q_{Vh}+q_{VT}+q_{Va})-S\\ &= \rho_L\frac{\partial}{\partial z}\left[K\left(\frac{\partial h}{\partial z}+1\right)+D_{TD}\frac{\partial T}{\partial z}+\frac{K}{Y_w}\frac{\partial P_g}{\partial z}\right]\\ &\quad+\frac{\partial}{\partial z}\left[D_{Vh}\frac{\partial h}{\partial z}+D_{VT}\frac{\partial T}{\partial z}+D_{Va}\frac{\partial P_g}{\partial z}\right]-S\end{aligned} \tag{B1}$$

where ρ_L, ρ_V, and ρ_i (kg m^{-3}) are the densities of liquid water, water vapor, and ice, respectively; θ_L, θ_V, and θ_i (m^3 m^{-3}) are the volumetric water content (liquid, vapor and ice, respectively); z (m) is the vertical space coordinate (positive upward); S (s^{-1}) is the sink term for the root water extraction. K (m s^{-1}) is hydraulic conductivity; h (m) is the pressure head; T (°C) is the soil temperature; and P_g (Pa) is the mixed pore-air pressure. γ_W (kg·m^{-2}·s^{-2}) is the specific weight of water. D_{TD} (kg·m^{-1}·s^{-1}·°C^{-1}) is the transport coefficient for adsorbed liquid flow due to temperature gradient; D_{Vh} (kg·m^{-2}·s^{-1}) is the isothermal vapor conductivity; and D_{VT} (kg·m^{-1}·s^{-1}·°C^{-1}) is the thermal vapor diffusion coefficient. D_{Va} is the advective vapor transfer coefficient (Zeng et al., 2011a, 2011b). q_{Lh}, q_{LT}, and q_{La}, (kg·m^{-2}·s^{-1}) are the liquid water fluxes driven by the gradient of matric potential $\frac{\partial h}{\partial z}$, temperature $\frac{\partial T}{\partial z}$, and air pressure $\frac{\partial P_g}{\partial z}$, respectively. q_{Vh}, q_{VT}, and q_{Va} (kg m^{-2} s^{-1}) are the water vapor fluxes driven by the gradient of matric potential $\frac{\partial h}{\partial z}$, temperature $\frac{\partial T}{\partial z}$, and air pressure $\frac{\partial P_g}{\partial z}$, respectively.

B.2. Dry Air Transfer

$$\frac{\partial}{\partial t}[\varepsilon\rho_{da}(S_a+H_cS_L)]=\frac{\partial}{\partial z}\left[D_e\frac{\partial\rho_{da}}{\partial z}+\rho_{da}\frac{S_aK_g}{\mu_a}\frac{\partial P_g}{\partial z}-H_c\rho_{da}\frac{q_L}{\rho_L}+\left(\theta_aD_{Vg}\right)\frac{\partial\rho_{da}}{\partial z}\right] \tag{B2}$$

where ε is the porosity; ρ_{da} (kg m^{-3}) is the density of dry air; S_a ($=1-S_L$) is the degree of air saturation in the soil; S_L ($=\theta_L/\varepsilon$) is the degree of saturation in the soil; H_c is Henry's constant; D_e (m^2 s^{-1}) is the molecular diffusivity of water vapor in soil; K_g (m^2) is the intrinsic air permeability; μ_a (kg m^{-2} s^{-1}) is the air viscosity; and D_{Vg} (m^2 s^{-1}) is the gas phase longitudinal dispersion coefficient

B.3. Energy Transfer

$$\begin{aligned}&\frac{\partial}{\partial t}[(\rho_s\theta_sC_s+\rho_L\theta_LC_L+\rho_V\theta_VC_V+\rho_{da}\theta_aC_a+\rho_i\theta_iC_i)(T-T_r)+\rho_V\theta_VL_0-\rho_i\theta_iL_f]-\rho_LW\frac{\partial\theta_L}{\partial t}\\ &=\frac{\partial}{\partial z}\left(\lambda_{eff}\frac{\partial T}{\partial z}\right)-\frac{\partial}{\partial z}[q_LC_L(T-T_r)+q_V(L_0+C_V(T-T_r))+q_aC_a(T-T_r)]-C_LS(T-T_r)\end{aligned} \tag{B3}$$

C_s, C_L, C_V, C_a, and C_i (J·kg^{-1}·°C^{-1}) are the specific heat capacities of solids, liquid, water vapor, dry air, and ice, respectively; ρ_s (kg m^{-3}) is the density of solids; θ_s, θ_a($=\theta_V$) is the volumetric fraction of solids and dry air in the soil; T_r (°C) is the reference temperature; L_0 (J kg^{-1}) is the latent heat of vaporization of water at temperature T_r; L_f (J kg^{-1}) is the latent heat of fusion; W (J kg^{-1}) is the differential heat of wetting (the amount of heat released when a small amount of free water is added to the soil matrix); and λ_{eff} (W·m^{-1}·°C^{-1}) is the effective thermal conductivity of the soil; q_L, q_V, and q_a (kg·m^{-2}·s^{-1}) are the liquid, vapor water flux, and dry air flux; S (s^{-1}) is the sink term of root water uptake.

Table B1
Properties of Soil Constituents (de Vries, 1963)

Substance	j	λ_j (mcal·cm^{-1} s^{-1}·°C^{-1})	C_j (mcal·cm^{-1}·s^{-1}·°C^{-1})	ρ_j (g cm^{-3})	g_j
Water	1	1.37	1	1	—
Air	2	0.06	0.0003	0.00125	—
Quartz	3	21	0.48	2.66	0.125
Clay minerals	4	7	0.48	2.65	0.125
Organic matter	5	0.6	0.6	1.3	0.5
Ice	6	5.2	0.45	0.92	0.125

B.4. Hydraulic Conductivity

According to Mualem (1976), the unsaturated hydraulic conductivity using Clapp and Hornberger, van Genuchten method can be expressed as

$$\mathrm{K_{Lh}} = \mathrm{K_s}(\theta/\theta_\mathrm{s})^{3+2/\beta} \tag{B4}$$

$$K_{Lh} = K_s S_e^l \left[1-\left(1-S_e^{1/m}\right)^m\right]^2 \tag{B5a}$$

$$S_e = \frac{\theta-\theta_r}{\theta_s-\theta_r} \tag{B5b}$$

where K_{Lh} and K_s (m s^{-1}) are the hydraulic conductivity and saturated hydraulic conductivity. $\beta(=1/b)$ is the empirical Clapp and Hornberger parameter. S_e is the effective saturation. l, n, and $m(=1-1/n)$ are the van Genuchten fitting parameters. The blocking effect of ice presence is estimated by the impedance factor,

$$K_{\mathrm{fLh}} = 10^{-\mathrm{EQ}} K_{\mathrm{Lh}} \tag{B6a}$$

$$Q = (\rho_i\theta_i/\rho_L\theta_L) \tag{B5b}$$

where K_{fLh} (m s^{-1}) is the hydraulic conductivity in frozen soils, K_{Lh} (m s^{-1}) is the hydraulic conductivity in unfrozen soils at the same negative pressure or liquid moisture content, Q is the mass ratio of ice to total water, and E is the empirical constant that accounts for the reduction in permeability due to the formation of ice (Hansson et al., 2004).

B.5. Thermal Conductivity

$$\lambda_{\mathrm{eff}} = \left(\sum_{j=1}^{6} k_j\theta_j\lambda_\mathrm{j}\right)\left(\sum_{j=1}^{6} k_j\theta_j\right)^{-1} \tag{B7}$$

where k_j is the weighting factor for each component; θ_j the volumetric fraction of the jth constituent; λ_j (W·m^{-1}·°C^{-1}) the thermal conductivity of the jth constituent. The six components are (1) water, (2) air, (3) quartz particles, (4) clay minerals, (5) organic matter, and (6) ice (see Table B1).

$$k_j = \frac{2}{3}\left[1+\left(\frac{\lambda_\mathrm{j}}{\lambda_1}-1\right)g_\mathrm{j}\right]^{-1} + \frac{1}{3}\left[1+\left(\frac{\lambda_\mathrm{j}}{\lambda_1}-1\right)\left(1-2g_\mathrm{j}\right)\right]^{-1} \tag{B8}$$

and g_j is the shape factor of the jth constituent (see Table B1), of which the shape factor of the air g_2 can be determined as follows,

$$g_2 = \begin{cases} 0.013 + \left(\dfrac{0.022}{\theta_{\mathrm{wilting}}} + \dfrac{0.298}{\theta_s}\right)\theta_L, & \theta_L < \theta_{\mathrm{wilting}} \\ 0.035 + \dfrac{0.298}{\theta_s}\theta_L, & \theta_L \geq \theta_{\mathrm{wilting}} \end{cases} \tag{B9}$$

Appendix C: Abbreviations

CFoC	Cumulative fraction of counts
COSMIC	Cosmic-ray Soil Moisture Interaction Code
CRNP	Cosmic-ray neutron probe
DA	Data assimilation
FT	Freezing-Thawing
LUT	Look-up table
L/USWC	Liquid/Unfrozen soil water content
N_0	Site-specific CRNP parameter
N_{he}	High-energy COSMIC parameter
OL	Open loop
OSSE	Observing System Simulation Experiment
PF	Particle filter
SFCC	Soil freezing characteristic curve
SIC	Soil ice content
SIR-PF	Sequential importance resampling—particle filter
SM/SWC	Soil moisture/Soil water content
STEMMUS	Simultaneous Transfer of Energy Mass and Momentum in the Unsaturated Soil
ST	Soil temperature
SWRC	Soil water retention curve
TSWC	Total soil water content

Acknowledgments
This work is supported by the National Natural Science Foundation of China (grant no. 41971033), the Netherlands Organisation for Scientific Research (NWO) (grant no. ENWWW.2018.5), and the ITC MSc thesis excellence program. Data used in this study can be found in the 4TU.Center for Research Data repository (https://doi.org/10.4121/uuid:3131b711-52f5-457f-a8dc-f73d4078ef2d). The authors thank the Editors and the anonymous referees for their valuable comments and suggestions.

References

Baatz, R., Bogena, H. R., Hendricks Franssen, H.-J., Huisman, J. A., Montzka, C., & Vereecken, H. (2015). An empirical vegetation correction for soil water content quantification using cosmic ray probes. *Water Resources Research*, *51*(4), 2030–2046. https://doi.org/10.1002/2014WR016443

Baatz, R., Bogena, H. R., Hendricks Franssen, H.-J., Huisman, J. A., Qu, W., Montzka, C., & Vereecken, H. (2014). Calibration of a catchment scale cosmic-ray probe network: A comparison of three parameterization methods. *Journal of Hydrology*, *516*, 231–244. https://doi.org/10.1016/j.jhydrol.2014.02.026

Babaeian, E., Sadeghi, M., Jones, S. B., Montzka, C., Vereecken, H., & Tuller, M. (2019). Ground, proximal and satellite remote sensing of soil moisture. *Reviews of Geophysics*, *57*. https://doi.org/10.1029/2018RG000618

Bogena, H. R., Huisman, J. A., Baatz, R., Hendricks Franssen, H. J., & Vereecken, H. (2013). Accuracy of the cosmic-ray soil water content probe in humid forest ecosystems: The worst case scenario. *Water Resources Research*, *49*(9), 5778–5791. https://doi.org/10.1002/wrcr.20463

Cherkauer, K. A., & Lettenmaier, D. P. (1999). Hydrologic effects of frozen soils in the upper Mississippi River basin. *Journal of Geophysical Research Atmospheres*, *104*(D16), 19,599–19,610. https://doi.org/10.1029/1999JD900337

Civan, F. (2000). Unfrozen water in freezing and thawing soils: Kinetics and correlation. *Journal of Cold Regions Engineering*, *14*(3), 146–156. https://doi.org/10.1061/(ASCE)0887-381X(2000)14:3(146)

Cox, P. M., Betts, R. A., Jones, C. D., & Spall, S. A. (2000). Acceleration of global warming due to carbon-cycle feedbacks in a coupled climate model. *Nature*, *408*(6809), 184–187. https://doi.org/10.1038/35041539

Dall'Amico, M. (2010). Coupled water and heat transfer in permafrost modeling. University of Trento. Retrieved from http://eprints-phd.biblio.unitn.it/335/1/Matteo_PhD_20100402.pdf

Dente, L., Vekerdy, Z., Wen, J., & Su, Z. (2012). Maqu network for validation of satellite-derived soil moisture products. *International Journal of Applied Earth Observation and Geoinformation*, *17*(1), 55–65. https://doi.org/10.1016/j.jag.2011.11.004

Desilets, D., Zreda, M., & Ferré, T. P. A. (2010). Nature's neutron probe: land surface hydrology at an elusive scale with cosmic rays. *Water Resources Research*, *46*(11), 1–7. https://doi.org/10.1029/2009WR008726

de Vries, D. A. (1963). Thermal properties of soils. In W. R. van Wijk (Ed.), *Physics of Plant Environment* (pp. 210–235). Amsterdam: North-Holland Publishing Co.

Draper, C., Mahfouf, J. F., Calvet, J. C., Martin, E., & Wagner, W. (2011). Assimilation of ASCAT near-surface soil moisture into the SIM hydrological model over France. *Hydrology and Earth System Sciences*, *15*(12), 3829–3841. https://doi.org/10.5194/hess-15-3829-2011

Evensen, G. (1994). Sequential data assimilation with a nonlinear quasi-geostrophic model using Monte Carlo methods to forecast error statistics. *Journal of Geophysical Research*, *99*(C5), 10,143–10,162. https://doi.org/10.1029/94jc00572

Evensen, G. (2003). The Ensemble Kalman Filter: Theoretical formulation and practical implementation. *Ocean Dynamics*, *53*(4), 343–367. https://doi.org/10.1007/s10236-003-0036-9

Farouki, O. T. (1981). The thermal properties of soils in cold regions. *Cold Regions Science and Technology*, *5*(1), 67–75. https://doi.org/10.1016/0165-232X(81)90041-0

Franz, T. E., Zreda, M., Ferre, T. P. A., Rosolem, R., Zweck, C., Stillman, S., et al. (2012). Measurement depth of the cosmic ray soil moisture probe affected by hydrogen from various sources. *Water Resources Research*, *48*(8), 1–9. https://doi.org/10.1029/2012WR011871

Gordon, N. J., Salmond, D. J., & Smith, A. F. M. (1993). Novel approach to nonlinear/non-gaussian Bayesian state estimation. *IEE Proceedings, Part F: Radar and Signal Processing*, *140*(2), 107–113. https://doi.org/10.1049/ip-f-2.1993.0015

Han, X., Franssen, H. J. H., Rosolem, R., Jin, R., Li, X., & Vereecken, H. (2015). Correction of systematic model forcing bias of CLM using assimilation of cosmic-ray neutrons and land surface temperature: A study in the Heihe Catchment, China. *Hydrology and Earth System Sciences*, *19*(1), 615–629. https://doi.org/10.5194/hess-19-615-2015

Hansson, K., Šimůnek, J., Mizoguchi, M., Lundin, L., & van Genuchten, M. T. (2004). Water flow and heat transport in frozen soil: Numerical solution and freeze-thaw applications. *Vadose Zone Journal*, *3*(2), 693–704. https://doi.org/10.2136/vzj2004.0693

Hawdon, A., McJannet, D., & Wallace, J. (2014). Calibration and correction procedures for cosmic-ray neutron soil moisture probes located across Australia. *Water Resources Research*, *50*(6), 5029–5043. https://doi.org/10.1002/2013WR015138

Kalman, R. E. (1960). A new approach to linear filtering and prediction problems. *Journal of Basic Engineering*, *82*(1), 35–45. https://doi.org/10.1115/1.3662552

Köhli, M., Schrön, M., Zreda, M., Schmidt, U., Dietrich, P., & Zacharias, S. (2015). Footprint characteristics revised for field-scale soil moisture monitoring with cosmic-ray neutrons. *Water Resources Research*, *51*(7), 5772–5790. https://doi.org/10.1002/2015WR017169

Koopmans, R. W. R., & Miller, R. D. (1966). Soil freezing and soil water characteristic curves. *Soil Science Society of America Journal*, *30*(6), 680–685. https://doi.org/10.2136/sssaj1966.03615995003000060011x

Li, Q., Sun, S., & Xue, Y. (2010). Analyses and development of a hierarchy of frozen soil models for cold region study. *Journal of Geophysical Research*, *115*(D3), 1–18. https://doi.org/10.1029/2009JD012530

Mironov, V. L., Muzalevskiy, K. V., & Ruzicka, Z. (2016). Retrieving profile temperatures in a frozen topsoil near the TFS, Alaska, Based on SMOS brightness temperatures at the 1. 4-GHz frequency. *IEEE Transactions on Geoscience and Remote Sensing*, *54*(12), 7331–7338. https://doi.org/10.1109/TGRS.2016.2599272

Montzka, C., Moradkhani, H., Weihermüller, L., Franssen, H. J. H., Canty, M., & Vereecken, H. (2011). Hydraulic parameter estimation by remotely-sensed top soil moisture observations with the particle filter. *Journal of Hydrology*, *399*(3–4), 410–421. https://doi.org/10.1016/j.jhydrol.2011.01.020

Montzka, C., Pauwels, V., Franssen, H.-J., Han, X., & Vereecken, H. (2012). Multivariate and multiscale data assimilation in terrestrial systems: A review. *Sensors*, *12*(12), 16,291–16,333. https://doi.org/10.3390/s121216291

Moradkhani, H. (2008). Hydrologic remote sensing and land surface data assimilation. *Sensors*, *8*(5), 2986–3004. https://doi.org/10.3390/s8052986

Moradkhani, H., Hsu, K.-L., Gupta, H., & Sorooshian, S. (2005). Uncertainty assessment of hydrologic model states and parameters: Sequential data assimilation using the particle filter. *Water Resources Research*, *41*(5), 1–17. https://doi.org/10.1029/2004WR003604

Moradkhani, H., Sorooshian, S., Gupta, H. V., & Houser, P. R. (2005). Dual state-parameter estimation of hydrological models using ensemble Kalman filter. *Advances in Water Resources*, *28*(2), 135–147. https://doi.org/10.1016/j.advwatres.2004.09.002

Mualem, Y. (1976). A new model for predicting the hydraulic conductivity of unsaturated porous media. *Water Resources Research*, *12*(3), 513–522. https://doi.org/10.1029/WR012i003p00513

Patterson, D. E., & Smith, M. W. (1981). The measurement of unfrozen water content by time domain reflectometry: Results from laboratory tests. *Canadian Geotechnical Journal*, *18*(1), 131–144. https://doi.org/10.1139/t81-012

Peng, J. (2017). Application of cosmic-ray probe for the detection of freezing-thawing process over Tibetan Plateau *(MSc. Thesis)*. University of Twente. Retrieved from https://webapps.itc.utwente.nl/librarywww/papers_2017/msc/wrem/peng.pdf

Philip, J. R., & De Vries, D. A. (1957). Moisture movement in porous materials under temperature gradients. *Transactions American Geophysical Union*, *38*(2), 222–232. https://doi.org/10.1029/TR038i002p00222

Rautiainen, K., Lemmetyinen, J., Schwank, M., Kontu, A., Ménard, C. B., Mätzler, C., et al. (2014). Detection of soil freezing from L-band passive microwave observations. *Remote Sensing of Environment*, *147*, 206–218. https://doi.org/10.1016/j.rse.2014.03.007

Rosolem, R., Shuttleworth, W. J., Zreda, M., Franz, T. E., Zeng, X., & Kurc, S. A. (2013). The effect of atmospheric water vapor on neutron count in the cosmic-ray soil moisture observing system. *Journal of Hydrometeorology*, *14*(5), 1659–1671. https://doi.org/10.1175/JHM-D-12-0120.1

Savitzky, A., & Golay, M. J. E. (1964). Smoothing and differentiation of data by simplified least squares procedures. *Analytical Chemistry*, *36*(8), 1627–1639. https://doi.org/10.1021/ac60214a047

Schreiner-McGraw, A. P., Vivoni, E. R., Mascaro, G., & Franz, T. E. (2016). Closing the water balance with cosmic-ray soil moisture measurements and assessing their relation to evapotranspiration in two semiarid watersheds. *Hydrology and Earth System Sciences*, *20*(1), 329–345. https://doi.org/10.5194/hess-20-329-2016

Schrön, M., Köhli, M., Scheiffele, L., Iwema, J., Bogena, H. R., Lv, L., et al. (2017). Improving calibration and validation of cosmic-ray neutron sensors in the light of spatial sensitivity. *Hydrology and Earth System Sciences*, *21*(10), 5009–5030. https://doi.org/10.5194/hess-21-5009-2017

Schwank, M., Stähli, M., Wydler, H., Leuenberger, J., Mätzler, C., Member, S., & Flühler, H. (2004). Microwave L-band emission of freezing soil. *IEEE Transactions on Geoscience and Remote Sensing*, *42*(6), 1252–1261. https://doi.org/10.1109/TGRS.2004.825592

Sheshukov, A. Y., & Nieber, J. L. (2011). One-dimensional freezing of nonheaving unsaturated soils: Model formulation and similarity solution. *Water Resources Research*, *47*(11), 1–17. https://doi.org/10.1029/2011WR010512

Shuttleworth, J., Rosolem, R., Zreda, M., & Franz, T. (2013). The COsmic-ray Soil Moisture Interaction Code (COSMIC) for use in data assimilation. *Hydrology and Earth System Sciences*, *17*(8), 3205–3217. https://doi.org/10.5194/hess-17-3205-2013

Su, Z., Wen, J., Dente, L., Van Der Velde, R., Wang, L., Ma, Y., et al. (2011). The Tibetan Plateau Observatory of plateau scale soil moisture and soil temperature (Tibet-Obs) for quantifying uncertainties in coarse resolution satellite and model products. *Hydrology and Earth System Sciences*, *15*(7), 2303–2316. https://doi.org/10.5194/hess-15-2303-2011

Swinbank, R., & O'Neill, A. (1994). Quasi-biennial and semi-annual oscillations in equatorial wind fields constructed by data assimilation. *Geophysical Research Letters*, *21*(19), 2099–2102. https://doi.org/10.1029/94GL01743

Taylor, K. E. (2001). Summarizing multiple aspects of model performance in a single diagram. *Journal of Geophysical Research*, *106*(D7), 7183–7192. https://doi.org/10.1029/2000JD900719

Topp, G. C., Davis, J. L., & Annan, A. P. (1980). Electromagnetic determination of soil water content. *Water Resources Research*, *16*(3), 574–582. https://doi.org/10.1029/WR016i003p00574

van Genuchten, M. T. (1980). A closed form equation for predicting the hydraulic conductivity of unsaturated soils. *Soil Science Society of America Journal*, *44*, 892–898. https://doi.org/10.2136/sssaj1980.03615995004400050002x

Watanabe, K., & Wake, T. (2009). Measurement of unfrozen water content and relative permittivity of frozen unsaturated soil using NMR and TDR. *Cold Regions Science and Technology*, *59*(1), 34–41. https://doi.org/10.1016/j.coldregions.2009.05.011

Wen, J., Su, Z., Zhang, T., Tian, H., Zeng, Y., Liu, R., & Kang, Y. (2013). New evidence for the links between the local water cycle and the underground wet sand layer of a mega-dune in the Badain Jaran Desert, China. *Journal of Arid Land*, *6*(4), 371–377. https://doi.org/10.1007/s40333-014-0062-0

Yu, L., Zeng, Y., Wen, J., & Su, Z. (2018). Liquid-vapor-air flow in the frozen soil. *Journal of Geophysical Research: Atmospheres*, *123*(14), 7393–7415. https://doi.org/10.1029/2018JD028502

Zeng, Y. (2013). In Y. Zeng (Ed.), *Coupled dynamics in soil*, (1st ed.). Berlin, Heidelberg: Springer Berlin Heidelberg. https://doi.org/10.1007/978-3-642-34073-4

Zeng, Y., & Su, Z. (2013). Reply to comment by Binayak P. Mohanty and Zhenlei Yang on "A simulation analysis of the advective effect on evaporation using a two-phase heat and mass flow model". *Water Resources Research*, *49*, 7836–7840. https://doi.org/10.1002/2013WR013764

Zeng, Y., Su, Z., Van Der Velde, R., Wang, L., Xu, K., Wang, X., & Wen, J. (2016). Blending satellite observed, model simulated, and in situ measured soil moisture over Tibetan Plateau. *Remote Sensing*, *8*(3), 1–22. https://doi.org/10.3390/rs8030268

Zeng, Y., Su, Z., Wan, L., & Wen, J. (2011a). A simulation analysis of the advective effect on evaporation using a two-phase heat and mass flow model. *Water Resources Research*, *47*(10), 1–18. https://doi.org/10.1029/2011WR010701

Zeng, Y., Su, Z., Wan, L., & Wen, J. (2011b). Numerical analysis of air-water-heat flow in unsaturated soil: Is it necessary to consider airflow in land surface models? *Journal of Geophysical Research Atmospheres*, *116*(20), 1–18. https://doi.org/10.1029/2011JD015835

Zeng, Y., Su, Z., Wan, L., Yang, Z., Zhang, T., Tian, H., et al. (2009). Diurnal pattern of the drying front in desert and its application for determining the effective infiltration. *Hydrology and Earth System Sciences*, *13*, 703–714. https://doi.org/10.5194/hess-13-703-2009

Zeng, Y., Wan, L., Su, Z., & Saito, H. (2009). Diurnal soil water dynamics in the shallow vadose zone (field site of China University of Geosciences, China). *Environmental Geology*, *58*, 11–23. https://doi.org/10.1007/s00254-008-1485-8

Zhang, H., Franssen, H. J. H., Han, X., Vrugt, J. A., & Vereecken, H. (2017). Joint state and parameter estimation of two land surface models using the ensemble Kalman filter and the particle filter. *Hydrology and Earth System Sciences*, *21*(9), 4927–4958. https://doi.org/10.5194/hess-21-4927-2017

Zhao, T., Shi, J., Hu, T., Zhao, L., Zou, D., Wang, T., et al. (2017). Estimation of high-resolution near-surface freeze/thaw state by the integration of microwave and thermal infrared remote sensing data on the Tibetan Plateau. *Earth and Space Science*, *4*(8), 472–484. https://doi.org/10.1002/2017EA000277

Zheng, D., Van Der Velde, R., Su, Z., Booij, M. J., & Hoekstra, A. Y. (2014). Assessment of roughness length schemes implemented within the noah land surface model for high-altitude regions. *Journal of Hydrometeorology*, *15*(3), 921–937. https://doi.org/10.1175/JHM-D-13-0102.1

Zhou, X., Zhao, P., Chen, J., Chen, L., & Li, W. (2009). Impacts of thermodynamic processes over the Tibetan Plateau on the Northern Hemispheric climate. *Science in China, Series D: Earth Sciences*, *52*(11), 1679–1693. https://doi.org/10.1007/s11430-009-0194-9

Zhou, X., Zhou, J., Kinzelbach, W., & Stauffer, F. (2014). Simultaneous measurement of unfrozen water content and ice content in frozen soil using gamma ray attenuation and TDR. *Water Resources Research*, *50*(12), 9630–9655. https://doi.org/10.1002/2014WR015640

Zreda, M., Desilets, D., Ferré, T. P. A., & Scott, R. L. (2008). Measuring soil moisture content non-invasively at intermediate spatial scale using cosmic-ray neutrons. *Geophysical Research Letters*, *35*(21), 1–5. https://doi.org/10.1029/2008GL035655

Zreda, M., Shuttleworth, W. J., Zeng, X., Zweck, C., Desilets, D., Franz, T., & Rosolem, R. (2012). COSMOS: The COsmic-ray Soil Moisture Observing System. *Hydrology and Earth System Sciences*, *16*(11), 4079–4099. https://doi.org/10.5194/hess-16-4079-2012